THESIS FOR THE DEGREE OF DOCTOR OF PHILOSOPHY IN THERMAL AND FLUID DYNAMICS

LES stochastic modelling of cavitation with its applications in OpenFOAM

BOXIONG CHEN

Division of Combustion and Propulsion Systems
Department of Mechanics and Maritime Sciences
CHALMERS UNIVERSITY OF TECHNOLOGY
Göteborg, Sweden 2019

LES stochastic modelling of cavitation with its applications in OpenFOAM

Boxiong Chen

ISBN 978-91-7597-861-1

Copyright © Boxiong Chen, 2019.

Thesis for the degree of Doctor of Philosophy
ISSN 0346-718X
Serial number: 4542

Department of Mechanics and Maritime Sciences

Division of Combustion and Propulsion Systems
Chalmers University of Technology
SE-412 96 GÖTEBORG, Sweden
Phone: +46 (0)31-772 10 00

Author e-mail: chenb@chalmers.se

Chalmers Reproservice
Göteborg, Sweden 2019

LES stochastic modelling of cavitation with its applications in OpenFOAM

Boxiong Chen

Division of Combustion and Propulsion Systems, Chalmers University of Technology

ABSTRACT

Cavitation is a vaporization process that commonly happens in high pressure injector nozzles nowadays. It has been shown by previous studies that cavitation has a significant influence on the subsequent atomization process, the quality of which would in turn heavily affect the process of combustion. Injector nozzle designs nowadays are trending towards higher and higher injection pressure, making the knowledge on cavitation phenomena more and more relevant and necessary. Studies into cavitation phenomena have attracted a rapidly increasing amount of interest from both the academic and the industrial circle. However, due to the inherent difficulties, cavitation still renders itself a process that is hard to be quantified with the experimental facilities nowadays. On the computational side, some cavitation models have been developed and applied successfully. Lagrangian models have had much success in several studies. However, when it comes to applications of parallel computing, the inherent difficulty on computational load balancing could hinder the application of Lagrangian models in simulations of realistic injector nozzles. The Eulerian approach, on the other hand, is naturally conducive to a better computational load balance, for which a simple domain decomposition usually suffices. In the category of Eulerian modeling, the homogeneous equilibrium model (HEM) imposes less of a requirement to computational load, thus have been widely used in applications nowadays.

As much as HEMs have been widely applied in both academic studies and commercial computational tools, the stochastic feature of cavitation phenomena has been missing in the single Eulerian field models nowadays. With only one Eulerian field, only one bubble radius associated with the volume fraction is solved in any spatial location. However, physically, the vapor bubble sizes

are highly fluctuating, hence can better be described by a probability density function (PDF). In order to solve the evolution equation of the PDF, a Eulerian Stochastic Field (ESF) model is developed in this work. Multiple Eulerian fields are used to represent a distribution of cavitation bubble radii.

The ESF method has been previously applied for cavitation simulations only in the context of a compressible flow solver. However, the solution of the compressible form of the Navier-Stokes equation is known to be computationally expensive for low Mach number flow. Therefore, whether the ESF model can be applied in combination with a pressure-based solver became an interesting question. In this work, we coupled the ESF model to a pressure-based PISO algorithm, making the ESF model computationally efficient enough for studies of realistic injector nozzle geometries and standard operating conditions. Several simplified geometries, including one step-contraction throttle and two academic injector nozzle designs, are investigated using the novel cavitation model. Furthermore, we applied the ESF model on a realistic multi-hole injector geometry (spray G/G2 as defined by the Engine Combustion Network (ECN)) demonstrating that the ESF cavitation model can be applied in simulations of realistic nozzle injector geometries.

Keywords: Cavitation, Rayleigh-Plesset Equation, Homogeneous Equilibrium Model, Modelling, Simulation, OpenFOAM, Eulerian Stochastic Field Method

Preface

Parts, but far from all, of the contributions presented in this thesis have previously been accepted to conferences or journals.

- **Boxiong Chen**, Zachary Falgout, Mark Linne, Michael Oevermann, "LES modelling of cavitation flow in a diesel injector nozzle," in *International Conference on Multiphase Flow*, Firenze, Italy, May 22nd to 27th, 2016.
- **Boxiong Chen**, Michael Oevermann, "An Eulerian stochastic field cavitation model coupled to a pressure based solver," in *Computers and Fluids*, 2018.
- **Boxiong Chen**, Michael Oevermann, "LES investigation of ECN spray G2 with an Eulerian stochastic field cavitation model," in *SAE World Congress Experience*, Detroit, USA, April 10 to 12, 2018.
- **Boxiong Chen**, Michael Oevermann, "LES investigation with an Eulerian stochastic field cavitation model," in *10th International Symposium on Cavitation*, Baltimore, USA, May 14 to 16, 2018.

Acknowledgments

First off, I am grateful to my advisor, Professor Michael Oevermann, for his genuine interest into science, and all the insightful discussions we had, which has finally built up to this thesis. Without our common persistence to physical sense, and the affluent time he allowed for the fundamentals, the work could have withered at many times when major problems presented themselves.

A thanks goes to the former head of the department, Ingemar Denbratt, head of the department Lucien Koopmans, and assistant Elenor Norberg, and all other fellow colleagues for making the combustion division a cozy and pleasant place to work in. Life could have been so much tougher, without assistance and guidance from the peers.

Also thank the Knut & Alice Wallenberg Foundation for the financial support involved in this project.

I would like to also thank many colleagues in Fluid Dynamics division, especially Håkan Nilsson, Xin Zhao, Ardalan Javadi, among others, for their invaluable experiences in OpenFOAM, and ICEM-CFD. Without their open-mindedness on sharing their expertise, siginificantly more work and time would have been needed to complete this work.

Boxiong Chen

Göteborg, January 2019

Contents

List of Figures

1

Introduction

1.1 Introduction

Fossil fuels are in general not renewable, and considering the resctriction on the available amount of oil, there could be a time of depletion. At present, the combustion of fossil fuels accounts for 80 percent of the energy consumption of today's world. Before the coming of any matured, and economically feasible solutions out of any of the new technologies to the energy issue, the only effective way to postpone such shortage is to use fossil fuel in a controlled and more efficient manner. From the environmental prospective, combustion gives off CO_2 as one of the major chemical product, which is vastly believed to be a

major cause of the global warming problem. In the less ideal load conditions where the combustion is insufficient, the process yields more harmful products such as CO and NO_x, unburned hydrocarbons and soot, which could give rise to severe health problems of human. Thus, it is necessary to reduce the consumption of fossil fuel and to improve combustion efficiency.

In the automotive engineering realm, researchers from both the industrial side and the academic side have been struggling hard to study the combustion inside the internal combustion engine from various aspects so as to meet the emission requirements. Among multiple factors, the quality of the fuel spray greatly affects the quality of combustion. Previous studies [1] have demonstrated that the cavitation that happens inside the needle following the passage contraction of flow enhances spray atomization, which in turn affects strongly the quality of subsequent combustion. And it is speculated that the enhancement is achieved by either inducing a direct disintegration locally, or through enhancing turbulence, which in turn, induces the breakup. Up to now, neither of the two mechanisms have got convincing validations from experiments or direct numerical simulations. More insight into the phenomena is required for both fundamental understanding of the process and to provide predictive simulations on relevant applications. However, it is commonly admitted that experimental study of cavitation on realistic nozzle geometries and injection conditions is difficult. As pointed out in [2], direct observation of cavities in realistic injectors requires high resolutions in both space and time, due to the small sizes and rapid evolvements of bubbles. Therefore previous experimental studies have mostly been performed on up-scaled nozzles, lower injection pressure and velocities with simple geometries. Results and conclusions obtained in such simplified designs could not be directly transfered to realistic injectors, they are rather used for validation and references for cavitation models.

Previous computational studies on cavitation with various levels of complexities have been carried out. Direct numerical resolving of the interface between phases could be computationally very expensive, and is therefore only feasible for fundamental studies. Various interface modelling methodologies have been

testified in previous studies. Although some of them have achieved good agreement with experiments, they would be less applicable to simulations of realistic nozzle geometries. Since we are more concerned about the applicability to real size, high pressure nozzle geometries, a homogeneous equilibrium mixture (HEM) model is adopted in the current work, which does not attempt to resolve or model the interface, but regard the bubbly flow as a mechanically and thermodynamically equilibrium mixture of fluid and gas. An alternative to HEM model, known as homogeneous relaxation model (HRM), assumes mechanical equilibrium between the two phases, but takes non-equilibrium phase change into account using a relaxation thermodynamic equilibrium. The interested reader is referred to [3] for a comparison of the two models. When it comes to modeling flash-boiling, which is driven by thermodynamic non-equilibrium, HRM has been successfully applied [4] and would be a better choice than HEM. However, cavitation happens mostly in a mechanical dominant regime of vaporization (more discussion on this point in Chapter 5). Therefore, we opt to save the computational cost by adopting HEM and further assume the mixture to be isothermal.

In a homogeneous equilibrium mixture, the phases can be represented by their volume fractions. In [5], an ordinary differential equation, commonly known as Rayleigh-Plesset equation, was developed to model the mass exchange between liquid and vapor phase under the assumption of spherical symmetry of bubbles. Models that solve one volume fraction combined with Rayleigh-Plesset models were first developed in [6, 7] and have gained much popularity in both commercial softwares and academic computations. However, given that more computational power has become available, Eulerian models that capture more physics are called for. As it is argued in [8], cavitation phenomenon is inheritantly a stochastic process, the complete states of which are unknown or inaccessible, because the sizes of vapor bubbles are subjected to fluctuations in the majority of applications. Single volume fraction model solves only one volume fraction, which corresponds to only one bubble radius per spatial location in an Eulerian field. Therefore, the fluctuating feature of realistic vapor bubbles is not reflected in single volume fraction model. In this work, a cavitation model based on the

probability density function (PDF) of the volume fraction is developed.

Mathematically, the most general form of PDF evolution equation is known as the Kramers-Moyal equation, as it will be discussed in more details in Chapter 3. The number of terms involved in Kramers-Moyal equation makes it impossible to model completely. However, an equation that contains only the first two terms of the Kramers-Moyal equation, named as Fokker-Planck equation, is significantly more convenient to model. Fortunately, the cancellation of terms higher than the 2nd order in Kramers-Moyal equation is justifiable under the assumption of a Markov process. The rationale behind this cancellation will be covered in more details in Chapter 3.

Although the Fokker-Planck equation is a much simpler formulation to model as compared to Kramers-Moyal equation, it is still a multi-dimensional partial differential equation, which is hard to solve. However, equivalent to the Fokker-Planck equation, a stochastic differential equation (SDE) can be formulated to describe the evolution of PDF. Moreover, SDEs can be solved using Monte Carlo type methods. The equivalence between the Fokker-Planck equation and SDE has been proved in previous studies and will be demonstrated in this thesis.

An SDE typically contains a deterministic part, which can be integrated using any classical integration schemes. The stochastic part of SDE however, introduces discontinuities hence requires a special numerical scheme. In Chapter 4, some fundamental theory on the derivation of stochastic integration schemes will be discussed, after which the stochastic Runge-Kutta 2nd order scheme (SRK2) is chosen for the model development. In the light of Monte Carlo method, multiple Eulerian fields are used to represent a PDF distribution of vapor bubbles in solving practice. Then, the stochastic numerical integration evolves the PDF according to the SDE that corresponds to the cavitation problem. The model that features this PDF solving procedure is known as Eulerian Stochastic Field (ESF) method.

Although the ESF method has been applied in [8] on cavitation modeling, the stochastic model was coupled to a compressible solver, which typically requires

a significant amount of computational time. In order to make the ESF method applicable to the simulations of realistic injector nozzles, a ESF method is applied in combination with a pressure based solver in this work, which greatly slackens the requirement on computational time. Also, a forth order Runge-Kutta method was used in [8] to solve the deterministic part of the stochastic model. The high computational cost involved in 4th order RK method, however, was wasted when it was combined with a first-order treatment in stochastic integration. As it has already been mentioned, we applied a second order stochastic Runge-Kutta method to perform the necessary stochastic numerical integration in this work. To the best knowledge of ours, this is the first computational cavitation study that couples ESF model with pressure based solver and applies high order stochastic numerical scheme. This is also the first application of the ESF model on the flow inside a complex multi-hole injector geometry, which will be discussed in details in Chapter 5.

Bibliography

[1] Akira Sou, Shigeo Hosokawa, and Akio Tomiyama, "Effects of cavitation in a nozzle on liquid jet atomization," *International Journal of Heat and Mass Transfer*, vol. 50, no. 17, pp. 3575–3582, 2007.

[2] Cyril Mauger, Loïc Méès, Marc Michard, Alexandre Azouzi, and Stéphane Valette, "Shadowgraph, schlieren and interferometry in a 2D cavitating channel flow," *Experiments in Fluids*, vol. 53, no. 6, pp. 1895–1913, 2012.

[3] M Palacz, M Haida, J Smolka, AJ Nowak, and A Hafner, "A comparison of homogeneous equilibrium and relaxation model for co2 expansion inside the two-phase ejector," in *Journal of Physics: Conference Series*. IOP Publishing, 2016, vol. 745, p. 032158.

[4] David P Schmidt, S Gopalakrishnan, and Hrvoje Jasak, "Multi-dimensional simulation of thermal non-equilibrium channel flow," *International journal of multiphase flow*, vol. 36, no. 4, pp. 284–292, 2010.

[5] Lord Rayleigh, "On the pressure developed in a liquid during the collapse of a spherical cavity, VIII.," *The London, Edinburgh, and Dublin Philosophical Magazine and Journal of Science*, vol. 34, no. 200, pp. 94–98, 1917.

[6] Weixing Yuan, Jürgen Sauer, and Günter H Schnerr, "Modeling and computation of unsteady cavitation flows in injection nozzles," *Mécanique & Industries*, vol. 2, no. 5, pp. 383–394, 2001.

[7] Weixing Yuan and Günter H Schnerr, "Numerical simulation of two-phase flow in injection nozzles: Interaction of cavitation and external jet formation," *Journal of Fluids Engineering*, vol. 125, no. 6, pp. 963–969, 2003.

[8] J Dumond, F Magagnato, and A Class, "Stochastic-field cavitation model," *Physics of Fluids*, vol. 25, no. 7, pp. 073302, 2013.

2

Cavitation and multiphase modelling

2.1 Introduction

In this chapter, the physics and modelling aspects of cavitation are discussed. An overview of some previous cavitation modelling studies will be given. What then follows is a description of the cavitation model in the current work.

2.2 Cavitation modelling: an overview

Cavitation is a vaporisation of a liquid following a drastic pressure drop below the vapour pressure. The transition from liquid to vapour can be achieved by either heating the liquid at a constant pressure, which is known as boiling, or through decreasing the pressure below the vapour pressure while maintaining constant temperature, which is known as cavitation. The two vaporization phenomena are shown in p-T diagram in Figure 2.1.

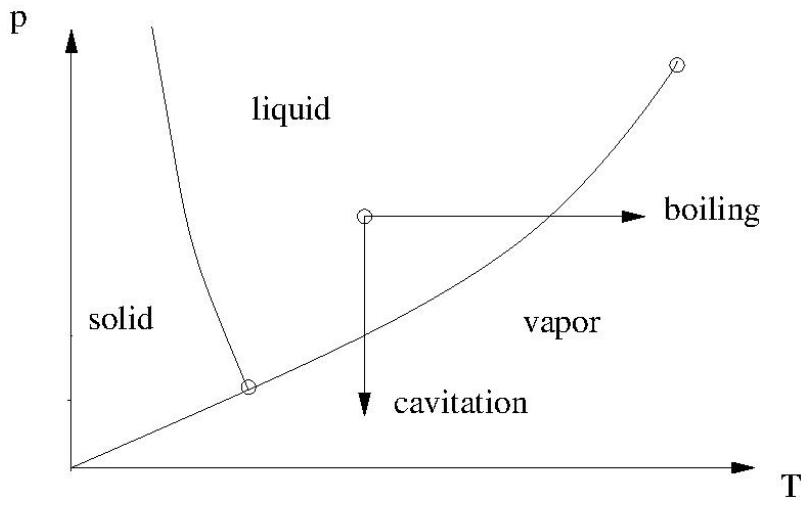

Figure 2.1: Cavitation and boiling demonstrated in p-T diagram

The cavitation processes could present itself in many engineering applications. For example, in hydraulic applications like pumps and marine propellers, the rapid growth and collapse of cavity bubbles could chip off the turbomachinery over time; in water treatment, the same phenomena incurred by bubbles could be harnessed to break the pollutant particles. Specifically in spray nozzles of internal combustion engines, previous studies have found that cavitation phenomena helps in breaking up liquid fuel spray which is important to proper fuel-air mixing and reduce the formation of pollutant. Therefore, cavitation at-

tracts substantial interests from both the automobile industry and the research side.

The influence of cavitation in injector nozzles on spray formation and breakup has been investigated both experimentally and computationally by previous works. Sou in [1] have demonstrated that the cavitation inside the fluid passage strongly affects the quality of the subsequent combustion. Whereas it remains an open question whether it enhances spray disintegration by contributing to the turbulent kinetic energy or by inducing a direct breakup mechanism locally. Experimental studies of cavitation on realistic nozzle geometries and injection conditions are difficult to perform. The geometric size and the residence time of the bubbles requires restrictively high resolutions of both time and space of optical access, for this reason, many experimental studies thus far have been based on up-scaled nozzles and low pressure conditions.

Computational studies with various modelling methodologies have been carried out. On the basis of Lagrangian approach, a Lagrangian description of individual bubbles or bubble clusters can be used to represent cavities, see, for instance, [2] and [3]. The interaction between bubbles, and bubble-wall interactions are modelled. On the Eulerian interface resolving side, both the liquid phase and the vapour phase are described by Eulerian fields. Since directly resolving interface normally takes formidably high computational cost, the treatment of interface is critical for Eulerian methods. [4] and [5] applied a level set method to represent the phase boundary between liquid and vapour phase. The onset of cavitation is identified when the maximum tensile stress exceeds a critical value. Based on this assumption a model of the sub-grid shape of the interface is applied. The curvature of the interface is then used to calculate surface tension forces in the momentum equation. Marcer and LeGouez in [6] applied a volume of fluids (VOF) method, reconstructed the interface with planes of arbitrary orientations in each cell. In the above mentioned studies, the sub-grid shape of interface is considered either by geometrical reconstruction or direct modelling. Methods of this kind fit well into fundamental studies of the behaviour of few bubbles. A more macroscopic class of models, called “interface

diffuse models" [7], regard bubbly flow as a continuous dispersed phase. The approach spends no effort tracking the fronts of each individual bubbles, but regard the bubbly flow as a mixture instead. The phases are represented by volume fractions, and the interface is treated as a zone where two phases coexists. Since physically bubbles exist on the sub-grid level, the volume fraction field does not define a sharp interface between the phases but provides the volumetric fraction of liquid and vapour within a computational cell. In the category of interface diffuse models, the number of equations that are used to describe the two phase further subcategorise different models. [8] proposed a seven equation model that consists of a conservative set of equations for mass, momentum, and energy for each of the two phases and an additional transport of equation for the volume fraction. Six-equation model by [9], [10], and [11] consist of the conservation equations for both phases, but only one pressure is kept assuming either incompressibility of one of the phases, or pressure equilibrium between the two phases. This approach reduced the computational cost involved in solving a volume fraction transport equation at the expense of a reduced validity on problems where transient wave propagation is important. Based on the seven-equation models, a five-equation model was derived in [12], assuming a mechanical equilibrium between the two phases. It involves transport of volume fraction, one set of momentum and energy equation, but two phase balance equations. [7] applied a discrete equation method (DEM) and a splitting method on the five-equation model to preserve the positivity of the solution and reduce the computational cost at the same time. The even simpler models make equilibrium assumption for both pressure and temperature in the different phases, thereby regarding the two phases practically as one. [13] and [14] applied the volume of fluids method, combined with a $k - \omega$ turbulence model to describe the flow field. The Rayleigh-Plesset relation was used to provide a source term for the volume fraction equation.

In the grand scheme of homogeneous mixture models, two particular type of models have gained their popularity in academic and commercial computational tools. Under the isothermal assumption, the first type of models assumes a barotropic equation of state (EOS), which provides a relationship between den-

sity and pressure. Coupled with pressure and velocity equations, the barotropic EOS indirectly controls the phase change through the density. The second type of models solve an equation of volume fraction, which is a direct indicator of phase change. Mass transfer models take effect in the gas/liquid volume fraction equation as source or sink terms. In the discussion below we will give a brief introdution to both of these types of models. In the discussion that follows, the two types of models will be refered to as "barotropic" and "mass transfer" models, respectively.

2.3 Barotropic cavitation model

2.3.1 Barotropic equation of state

We start the discussion with the barotropic equation of state for superheated vapor and compressed liquid:

$$\rho_v = \psi_v p, \tag{2.1}$$

$$\rho_l = \rho_l^0 + \psi_l p, \tag{2.2}$$

where ψ_l and ψ_v denote the speeds of sound of liquid and vapor phase, respectively. The ρ_l^0 in Eqn.(2.2) is a constant. Eqn.(2.2) represents a linear density-pressure relationship in the liquid phase.

A vapor fraction, an indicator of phase change, can be defined as follow:

$$\gamma = \frac{\rho - \rho_{l,sat}}{\rho_{v,sat} - \rho_{l,sat}} \tag{2.3}$$

where $\rho_{l,sat}$ and $\rho_{v,sat}$ denote the densities of liquid and vapor at saturation point.

An equilibrium equation of state can be assumed for the mixture as follow:

$$\rho = (1-\gamma)\rho_l^0 + (\gamma\psi_v + (1-\gamma)\psi_l)p_{sat} + \psi(\gamma)(p - p_{sat}) \tag{2.4}$$

Commonly applied models of $\psi(\gamma)$ are:

- Wallis model [15]

$$\psi_{Wallis} = (\gamma\rho_{v,sat}+(1-\gamma)\rho_{l,sat})\left(\gamma\frac{\psi_v}{\rho_{v,sat}}+(1-\gamma)\frac{\psi_l}{\rho_{l,sat}}\right), \quad (2.5)$$

- Chung model [16]

$$s_{fa} = \frac{\frac{\rho_{v,sat}}{\psi_v}}{(1-\gamma)\frac{\rho_{v,sat}}{\psi_v}+\gamma\frac{\rho_{l,sat}}{\psi_l}}, \quad (2.6)$$

$$\psi_{Chung} = \left((\frac{1-\gamma}{\sqrt{\psi_v}}+\frac{\gamma s_{fa}}{\sqrt{\psi_l}})\frac{\psi_v\psi_l}{s_{fa}}\right)^2, \quad (2.7)$$

- linear model

$$\psi_{linear} = \gamma\psi_v + (1-\gamma)\psi_l. \quad (2.8)$$

2.3.2 Governing equations

A momentum equation of the mixture is solved, which can be written as

$$\frac{\partial\rho\vec{u}}{\partial t} + \nabla(\rho\vec{u}\vec{u}) = \nabla\cdot(\mu\nabla\vec{u}) - \nabla p. \quad (2.9)$$

where $\vec{u}$ and p denote velocity vector and pressure in an Eulerian field. ρ and μ denote density and dynamic viscosity of the mixture, which are defined as:

$$\rho = (1-\alpha_l)\rho_v + \alpha_l\rho_l, \quad (2.10)$$

$$\mu = (1-\alpha_l)\rho_v\nu_v + \alpha_l\rho_l\nu_l, \quad (2.11)$$

where ρ_l, ν_l and ρ_v, ν_v denote the density and kinematic viscosity of the liquid phase and the vapor phase, respectively.

The mass conservation of the mixture can be expressed as

$$\frac{\partial\rho}{\partial t} + \nabla\cdot(\rho\vec{u}) = 0, \quad (2.12)$$

which is used twice in the implementation of cavitatingFoam. Once as a redundant equation to solve mixture density ρ. With known density, the vapor

fraction γ can be calculated from equation (2.3). The reason why we describe it as "redundant" is because, Eqn (2.12) is enforced again to in order to solve pressure later on in the solving sequence as follow

$$\frac{\partial \psi p}{\partial t} - (\rho_l^0 + (\psi_l - \psi_v)p_{sat})\frac{\partial \gamma}{\partial t} - p_{sat}\frac{\partial \psi}{\partial t} + \nabla \cdot (\rho \vec{u}) = 0. \tag{2.13}$$

The above equation can be derived if we plug the barotropic EOS (2.4) into the Eqn (2.12). In the solving sequence of cavitatingFoam, pressure p is the only implicit variable in the above equation.

2.4 Mass transfer cavitation model

2.4.1 Two phase equations

We start with the definition of volume fraction. As proposed in [17], the vapor in each control volume is assumed to consist of monodispersed spherical bubbles. Therefore the liquid volume fraction can be written as

$$\alpha_l = \frac{1}{1 + n * 4\pi R^3/3}, \tag{2.14}$$

where R denotes bubble radius and n is the number of nuclei per unit volume of fluid, which must be prescribed. The closure for α_l can be achieved by taking the material derivative:

$$\frac{\mathrm{d}\alpha_l}{\mathrm{d}t} = -3\alpha_l(1 - \alpha_l)\frac{\dot{R}}{R} \tag{2.15}$$

or

$$\dot{\alpha_l} + \vec{u} \cdot \nabla \alpha_l = -3\alpha_l(1 - \alpha_l)\frac{\dot{R}}{R} \tag{2.16}$$

A model for the bubble growth rate $\dot{R}$ (mass transfer between the two phases) is needed to close the equation above, which will be discussed in the next section.

It is worth mentioning that specific to the implementation in foam extended 3.1 (as well as many of other OpenFOAM releases), mass conservation equation

does not appear in exactly the form of Eqn. (2.12). Instead, if we try to reformulate Eqn. (2.12) into an equation that involves the divergence of $\vec{u}$, we get

$$\nabla \cdot \vec{u} = -\frac{1}{\rho}\frac{d\rho}{dt} \tag{2.17}$$

The reasoning behind the preference for the above formulation has something to do with some of the conventions of OpenFOAM development. Interested readers are highly encouraged to refer to the appendix for more details.

Note that we have Eqn. (2.10), which tells us density is a linear function of volume fraction. Plugging Eqn. (2.10) into the RHS of Eqn. (2.17), we get

$$\nabla \cdot \vec{u} = \frac{\rho_v - \rho_l}{\rho}\frac{d\alpha_l}{dt}. \tag{2.18}$$

The above equation reveals that the RHS of the divergence equation is equivalent to the RHS of volume fraction equation factored by a term of densities. Therefore, the closure of the RHS of the divergence equation can also be achieved with the selected mass transfer model.

The large eddy simulation work involved in this thesis requires a turbulence model for the subgrid turbulence. As it is the common practice of LES simulation, we solve a filtered momentum equation, as follow:

$$\frac{\partial}{\partial t}(\bar{\rho}\tilde{u}) + \nabla \cdot (\bar{\rho}\tilde{u}\tilde{u}) = \nabla \cdot (\mu_{eff}\nabla\tilde{u}) - \nabla\bar{p}, \tag{2.19}$$

where $\tilde{u}$ denotes Favre averaged velocity and $\bar{\rho}$, $\bar{p}$ Reynolds averaged density and pressure. μ_{eff} denotes effective viscocity, which is the combination of dynamic viscosity and turbulent viscosity:

$$\mu_{eff} = \mu + \mu_{turb}. \tag{2.20}$$

It is obvious that in order to close Eqn. (2.19), the closure of μ_{turb} needs to be achieved, which is the purpose of turbulence models. Under the framework of LES, a variety of turbulence models have been developed due to the continuous effort of CFD community. In the simulation of our work, we adopt Smagorinksy

model [18], which assumes that the energy production and dissipation of the sub-grid scales are in equilibrium. The turbulent kinematic viscosity is modeled as follow:

$$\nu_{turb} = (C_s \Delta_g)^2 \sqrt{2\tilde{S}_{ij}\tilde{S}_{ij}}, \tag{2.21}$$

where C_s is a constant and Δ_g represents grid size. S_{ij} is the filtered rate of strain tensor, which is calculated based on the local gradient of filtered velocity:

$$\tilde{S_{ij}} = \frac{1}{2}\left(\frac{\partial \tilde{U}_i}{\partial x_j} + \frac{\partial \tilde{U}_j}{\partial x_i}\right). \tag{2.22}$$

Our discussion so far has covered the derivation of momentum equation in both the original formulation and the filtered one. The divergence constraint has been given in Eqn. (2.18). Before delving into a massive discussion on the mass transfer model, namely the closure for the RHS of Eqn. (2.18), we will have a discussion on how the incompressible Navier-Stokes equation is solved.

2.4.2 Pressure velocity coupling and the PISO algorithm

In the last section, we derived the incompressible Navier-Stokes equation and the divergence constraint specific to cavitation problems. Solving such three-dimensional partial differential equations in a coupled way is usually limited to only cases of smaller problems. The most commonly used way to solve sush equation set is through a segregated approach (e.g. [19]), in which velocities and pressure are updated in sequence. The approach used in this work is commonly known as Pressure Implicit Split Operation (PISO) algorithm, which will be discussed below.

We start with the momentum equation. If we discretize the terms relevant to velocities and lump them together and leave pressure gradient term aside, we get:

$$\sum_i a_i U_i - \frac{U^0}{\Delta t} = -\nabla p, \tag{2.23}$$

where the a_i denotes the entries of matrix corresponding to the discretized momentum equation. $\sum_i a_i U_i$ includes the contributions from all the implicit velocity terms in a discretized momentum equation. U^0 represents the velocity from the previous time step and the second term on the LHS comes from time discretization of velocity. In order to rid ourselves from complex matrix manipulation (matrix inversions or decompositions), we can get the following equation, keeping only the diagonal terms as implicit:

$$a_P U_P = H(U) - \nabla p, \tag{2.24}$$

where

$$H(U) = -\sum_N a_N U_N + \frac{U^0}{\Delta t}. \tag{2.25}$$

$-\sum_N a_N U_N$ denotes the contribution of neighboring nodes and terms with subscript P represent the values associated with the cell under consideration. Note that high order schemes are not considered in this discussion, and the velocity values of neighboring nodes are essentially treated explicitly here. Now we take a look at the divergence constraint:

$$\nabla \cdot \vec{U} = S_v \left(\alpha_l^0, p^0\right). \tag{2.26}$$

where the $S_v(\alpha_l^0, p^0)$ denotes the volumetric source term contributed by the vaporization of liquid. In practice, pressure p and liquid volume fraction α_l are treated explicitly in the source terms in pressure equation, hence the superscripts "0". In the framework of finite volume method, flux needs to be considered for the purpose of discretization. According to Gauss theorem, Eqn. (2.26) can be rewritten as:

$$\nabla \cdot \vec{U} = \sum_f S \cdot U_f = S_v \left(\alpha_l^0, p^0\right), \tag{2.27}$$

where S denotes the vector of the surface of the control volume, whose directions are normal to the surface and U_f denotes velocity on the surface, which can be calculateded from interpolation of velocity on the grids. Eqn. (2.24) can

be rearranged to express velocity U:

$$U_P = \frac{H(U)}{a_P} - \frac{\nabla p}{a_P}. \tag{2.28}$$

Velocities on the cell faces can be obtained through interpolation of velocities in the cell:

$$U_f = \left(\frac{H(U)}{a_P}\right)_f - \left(\frac{\nabla p}{a_P}\right)_f. \tag{2.29}$$

Face values of velocities will be used to calculate face flux later on, which will, in turn, update the velocity equation in the PISO loop.

Imposing the constraint on the velocity vector in Eqn. (2.28), we obtain a Poisson equation for pressure:

$$\nabla \cdot \left(\frac{1}{a_P}\nabla p\right) = \nabla \cdot \left(\frac{H(U)}{a_P}\right) - S_v\left(\alpha_l^0, p^0\right). \tag{2.30}$$

Using Eqn. (2.29), face flux F can be calculated as:

$$F = S \cdot U_f = S \cdot \left[\left(\frac{H(U)}{a_P}\right)_f - \left(\frac{\nabla p}{a_P}\right)_f\right]. \tag{2.31}$$

Having obtained the momentum equation and pressure Poisson equation that are specific for numerical solutions, a solving loop in line with the PISO algorithm can be written as follow:

- Update the volume fraction equation with the pressure field obtained from the old time step.
- Solve Eqn. (2.28). At this point, the pressure field is still not updated. Therefore, the resulting velocity U would be only an aproximation of the new velocity field, which needs to be corrected later on. This step is commonly known as momentum predictor.
- The $H(U)$ can be assembled using the predicted velocities. Then we obtain a new pressure solution by solving the pressure Poisson equation (2.30).

- The velocity solution should be corrected in line with the new pressure solution. Therefore, we update the flux F in Eqn. (2.31) using the new pressure field, and then solve Eqn. (2.24) again. The last two solution-correction steps can be repeated till the errors reach the prescribed tolerances.

2.4.3 Mass transfer models

There have been numerous investigations since the beginning of the last century to achieve the closure of $\dot{R}$. Works on this term seek to model the mass transfer between the liquid and the vapor phase, which coincides with geometrical changes of the two phase zone. As such, a discussion on spherical bubble dynamics will be given first and Rayleigh-Plesset equation will be derived along with the discussion.

Spherical bubble dynamics and Rayleigh-Plesset equation

A thorough discussion on single spherical bubble dynamics is given in [20]. Here, a tailored recount will be given for the completeness of the discussion. Let us consider a spherical vapor bubble with radius $R(t)$ (see Figure 2.2), which varies with respect to time t in an infinite domain of liquid. The temperature and pressure in the liquid domain and far from the bubble are denoted as T_∞ and $p_\infty(t)$ respectively. We assume the density ρ_l and viscosity μ_l to be constants. To simplify, we will also exclude the internal flow of vapor from the discussion and consider the content inside the bubble as homogeneous. The temperature and pressure inside the bubble $T_b(t)$ and $p_b(t)$ are assumed to be uniform.

Mass conservation inside the bubble requires that

$$u(r,t) = \frac{F(t)}{r^2} \ (r < R) \tag{2.32}$$

where u denotes the velocity. $F(t)$ and $R(t)$ are related through a flux condition at the bubble surface, which will be considered next. The volume produc-

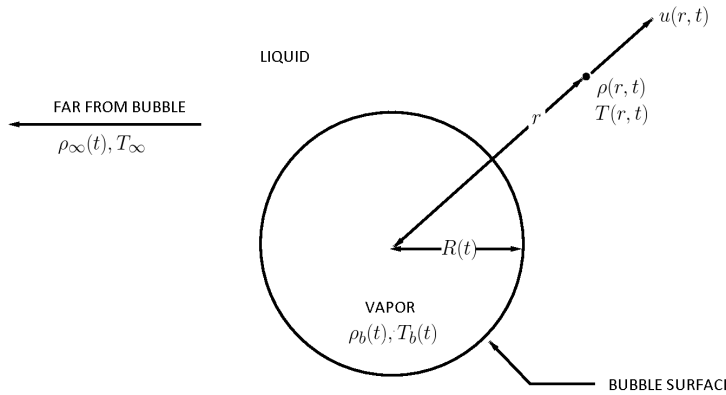

Figure 2.2: Schematic of a spherical bubble

tion rate of vapor at the bubble surface is $\rho_v(T_b)4\pi R^2\frac{dR}{dt}$. Mass conservation implies that the inward volume flux of liquid relative to the surface would be $\frac{\rho_v(T_b)}{\rho_l}4\pi R^2\frac{dR}{dt}$. In the majority of practical cases where $\rho_v(T_b) << \rho_l$ the inward volume flux of liquid becomes negligible as compared to the volume flux of vapor. This leads to $u(R,t) = \frac{dR}{dt}$. Hence we have

$$F(t) = R^2\frac{dR}{dt}. \tag{2.33}$$

Assuming that the liquid is Newtonian, the Navier Stokes equation in radial coordinate gives

$$\frac{\partial u}{\partial t} + u\frac{\partial u}{\partial r} = \nu_l\frac{1}{r^2}\frac{\partial}{\partial r}(r^2\frac{\partial u}{\partial r}) - \frac{1}{\rho_l}\frac{\partial p}{\partial r}. \tag{2.34}$$

Plugging in $u = \frac{F(t)}{r^2}$ into the Navier Stokes equation results in

$$-\frac{1}{\rho_l}\frac{\partial p}{\partial r} = \frac{1}{r^2}\frac{dF}{dt} - \frac{2F^2}{r^5} \tag{2.35}$$

and the viscous term vanishes. However, the effect of viscosity will play a role via the balance of stress at the bubble boundary. Integrating the equation above

with respect to radial position r, we have

$$\frac{p - p_\infty}{\rho_l} = \frac{1}{r}\frac{dF}{dt} - \frac{1}{2}\frac{F^2}{r^4}. \tag{2.36}$$

Here we have applied a boundary condition at the far field $p = p_\infty\Big|_{r=\infty}$.

Let us now consider a thin lamina that contains a segment of interface on the bubble boundary (see Figure 2.3). The net stress on this lamina in the radially outward direction is

$$\sigma_{rr}\Big|_{r=R} + p_b - \frac{2S}{R}, \tag{2.37}$$

where S denotes surface tension at the interface. Since $\sigma_{rr} = -p + 2\mu_l \frac{\partial u}{\partial r}$, at the interface we have

$$\begin{aligned}
\sigma_{rr}\Big|_{r=R} &= \Big(-p + 2\mu_l \frac{\partial u}{\partial r}\Big)_{r=R} \\
&= -p\Big|_{r=R} + 4\mu_l \frac{F}{r^3}\Big|_{r=R} \\
&= -p\Big|_{r=R} + \frac{4\mu_l}{R}\frac{dR}{dt}.
\end{aligned}$$

The net force per unit area on the interface contained in the lamina is

$$p_b - p\Big|_{r=R} - \frac{4\mu_l}{R}\frac{dR}{dt} - \frac{2S}{R}. \tag{2.38}$$

In the absence of mass transport across the interface this sum must be zero. Therefore, we have

$$p\Big|_{r=R} = \frac{4\mu_l}{R}\frac{dR}{dt} + p_b - \frac{2S}{R}. \tag{2.39}$$

Plugging the above equation of $p\Big|_{r=R}$ into Eqn.(2.36) and substituting $F(t)$ with $R^2\frac{dR}{dt}$ results in

$$\frac{p_b(t) - p_\infty}{\rho_l} = R\frac{d^2R}{dt^2} + \frac{3}{2}\Big(\frac{dR}{dt}\Big)^2 + \frac{4\nu_l}{R}\frac{dR}{dt} + \frac{2S}{\rho_l R}. \tag{2.40}$$

The above equation was first derived by Rayleigh (1917) and Plesset (1949) and it was applied to consider traveling cavitation bubbles. Thus, the equation

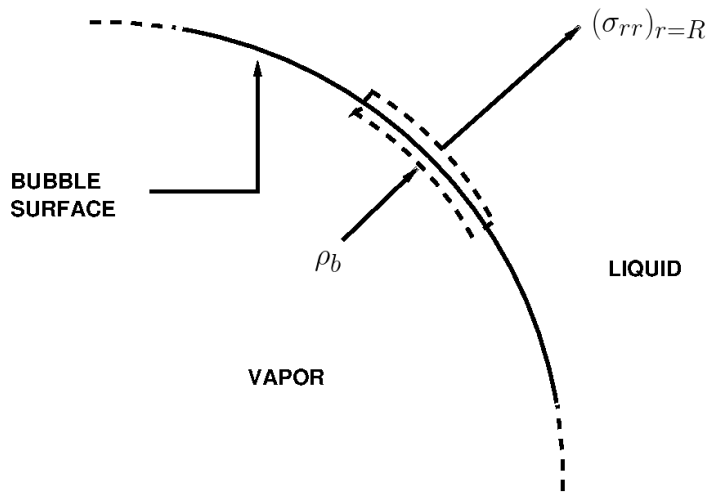

Figure 2.3: Portion of spherical bubble surface

is commonly known as Rayleigh-Plesset equation. In the section that follows, some further assumptions and simplifications of the above equation will be discussed, before the final formulation of the mass transfer model used in this work is presented.

Some simplifications and their viabilities

The pressure term on the LHS of Eqn.(2.40) requires knowledge of the pressure inside the bubble. If we assume that the bubble contains only vapor, then the pressure $p_b(t)$ will be equivalent to the vaporization pressure of the substance at a temperature T_b. Although a much more generalized assumption would take some quantity of contaminant gas into consideration, as it would better represent the contents in any realistic bubble, partial pressure associated with contaminant will be neglected in our discussion here. Interested readers are encouraged to find a discussion similar to this section without neglecting con-

taminant gas in [20], given a potentially major effect it might have on bubble dynamics. For now, with the pure vapor assumption on bubble content, we have

$$p_b(t) = p_v(T_b), \tag{2.41}$$

where T_b remains to be determined. Under some conditions, the unknown T_b departs little from the known T_∞. Thus, Eqn.(2.40) can be written into the following form:

$$\frac{p_v(T_\infty) - p_\infty(t)}{\rho_l} + \frac{p_v(T_b) - p_v(T_\infty)}{\rho_l} = R\frac{d^2R}{dt^2} + \frac{3}{2}\Big(\frac{dR}{dt}\Big)^2 + \frac{4\nu_l}{R}\frac{dR}{dt} + \frac{2S}{\rho_l R}. \tag{2.42}$$

The second term on the LHS is commonly referred to as "thermal term", which could possibly become more dominating than the first term under certain conditions. Therefore, an evaluation of the thermal term would be necessary. In [20], the thermal term is evaluated using a Taylor expansion. Neglecting terms higher than 1st order, the thermal term can be linearized as

$$\frac{p_v(T_b) - p_v(T_\infty)}{\rho_l} = \frac{1}{\rho_l}\frac{d\rho_v}{dT}(T_b - T_\infty), \tag{2.43}$$

where

$$\frac{d\rho_v}{dT} = \frac{\rho_v(T_\infty)L(T_\infty)}{T_\infty} \tag{2.44}$$

and L being a notation of latent heat.

Some further derivation involved in the evaluation of thermal term is omitted in the discussion here due to its complexity and lack of relevance to our purpose of introducing the model. However, it is found out that the thermal term scales with the thermodynamic parameter

$$\Sigma(T_\infty) = \frac{L^2\rho_v^2}{\rho_l^2 c_{p,l} T_\infty \alpha_l^{\frac{1}{2}}} \tag{2.45}$$

whose units are $m/s^{1.5}$. $c_{p,l}$ denotes constant pressure specific heat, and α_l denotes thermal diffusivity of liquid and confusion with volume fraction should be avoided.

In [20], a plot of Σ values for various saturated liquids as a function of the reduced temperature was provided, see Figure 2.4. By and large, it is safe to argue that thermal effect can be neglected when T_∞ is not expected to be too close to critical temperature in the cavitation problem under consideration.

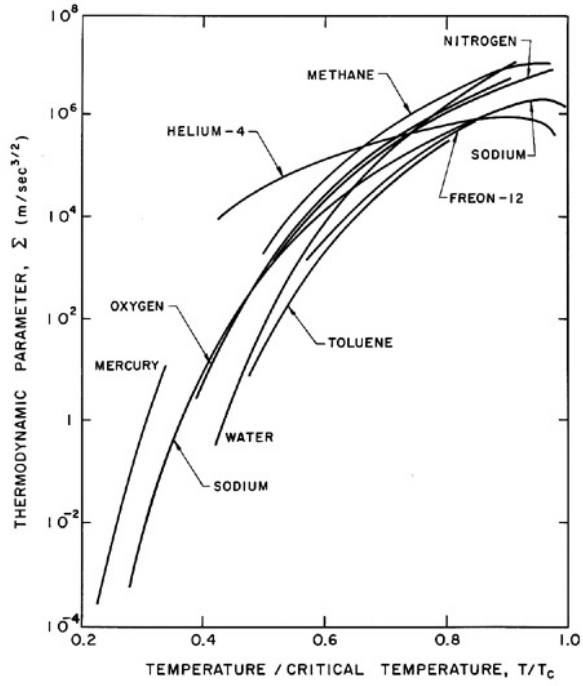

Figure 2.4: Values of the thermodynamic parameter, Σ, for various saturated liquids as a function of the reduced temperature, T/T_c.

An analytical solution to Rayleigh-Plesset equation is available in the case of a step function change in p_∞. Although this is a non-trivial limitation in a theoretical study, it presents a mode of pressure change that is highly relevant to CFD simulations, in which time is discrete. The analytical solution of such case is rather complicated, interested readers should refer to [20]. However, it is worth mentioning that the asymptotic solution of bubble growth can be obtained

from the analytical solution:

$$\dot{R} = \sqrt{\frac{2}{3}\frac{p_v - p_\infty}{\rho_l}}. \tag{2.46}$$

In CFD simulation practices, the asymtpotic solution above has served as a fairly convenient and robust model for the closure of $\dot{R}$. In an Eulerian-based model, $p_v(T_\infty)$ above is often replaced by the vaporization pressure corresponding to the local temperature, while the p_∞ is assumed to be local pressure. In the pure theoretical sense, this implies that the bubbles under consideration have to be far smaller than the control volume, which is probably violated sometimes in practical simulations (think about the situation where full cavitation spots exist in a domain). Also, a formula to calculate the duration time of the initial acceleration phase of bubble growth is proposed in [20]. However, how this time scale compares with typical simulation time steps has rarely been considered in practical CFD simulations. While it would be interesting to evaluate the effect of the above mentioned shortcomings of the model, the work involved would deviate too much from the scope of the current PhD project. Lastly, in [20], it is argued that a practical evaluation of bubble collapse can be hard to achieve with a spherical bubble analysis similar to the above. Aside from the absence of contaminant gas, typically a collapsing bubble would lose its spherical symmetry and the final stage of collapse could involve an extremely high velocity such that the incompressibility assumption may no longer hold. Considering such limitations, the bubble collapse models have not been considered in this work. We sincerely encourages future modeling studies to work on the development of physically sounded yet practically convenient models that address the above mentioned issues.

Equipped with the above closure for $\dot{R}$, the focus is then placed on solving Eqn (2.16). The solving framework that has been presented up to this point constitutes the methodology of several previous works, e.g., [14] [21], and cutting-edge solvers, e.g., interPhaseChangeFoam in OpenFOAM, which will be discussed again in the later chapters. It is obvious that, the single volume fraction field in this type of models corresponds to only one bubble radius per computational cell. However, with a reasonable resolution in CFD practice,

we should expect to observe a population of bubbles instead of just one bubble within any of the regions delimited by each cell. Thus, the description of such population amounts to a "population balance" problem, which has been studied in various branches of modern science, e.g., chemical engineering and biology. Among these branches, researchers in the area of combustion have developed several models that solves the probability density function (PDF) (a mathematical description of a population, more details will be covered in Chapter 3). Pope in [22] solved the PDF transport equation by tracking Lagrangian particles in combination with Monte-Carlo method in a combustion problem. The spatial position of each particle is included as one of the stochastic variables and evolves according to PDF equation. This approach, therefore, entails no Eulerian grids. In [23], a more Eulerian-based approach was developed. The particles reside on an Eulerian field, and moves from one node to another following rules that are based on transportation. In the current work, we adopt the full Eulerian framework as in [24, 25]. Following certain stochastic procedures, which will be discussed in the next chapter, an ensemble of Eulerian fields is generated to represent a distribution of radii in this work.

Bibliography

[1] Akira Sou, Shigeo Hosokawa, and Akio Tomiyama, "Effects of cavitation in a nozzle on liquid jet atomization," *International Journal of Heat and Mass Transfer*, vol. 50, no. 17, pp. 3575–3582, 2007.

[2] E Giannadakis, M Gavaises, and C Arcoumanis, "Modelling of cavitation in diesel injector nozzles," *Journal of Fluid Mechanics*, vol. 616, pp. 153–193, 2008.

[3] Emmanouil Giannadakis, *Modelling of cavitation in automotive fuel injector nozzles*, Ph.D. thesis, Imperial College London (University of London), 2005.

[4] Sadegh Dabiri, WA Sirignano, and DD Joseph, "Cavitation in an orifice flow," *Physics of Fluids*, vol. 19, no. 7, pp. 072112, 2007.

[5] S Dabiri, WA Sirignano, and DD Joseph, "A numerical study on the effects of cavitation on orifice flow," *Physics of Fluids*, vol. 22, no. 4, pp. 042102, 2010.

[6] R Marcer and JM LeGouez, "Simulation of unsteady cavitating flows in diesel injector with an improved VOF-method," in *17th ILASS-Europe Conf*, 2001.

[7] Maria Giovanna Rodio and Rémi Abgrall, "An innovative phase transition modeling for reproducing cavitation through a five-equation model and theoretical generalization to six and seven-equation models," *International Journal of Heat and Mass Transfer*, vol. 89, pp. 1386–1401, 2015.

[8] MR Baer and JW Nunziato, "A two-phase mixture theory for the deflagration-to-detonation transition (DDT) in reactive granular materials," *International Journal of Multiphase Flow*, vol. 12, no. 6, pp. 861–889, 1986.

[9] Mamoru Ishii, "Thermo-fluid dynamic theory of two-phase flow," *NASA STI/Recon Technical Report A*, vol. 75, pp. 29657, 1975.

[10] JA Boure and JM Delhaye, "General equations and two-phase flow modeling," *Handbook of multiphase systems*, pp. 1–36, 1982.

[11] Patrick Barry Butler, MF Lembeck, and H Krier, "Modeling of shock development and transition to detonation initiated by burning in porous propellant beds," *Combustion and Flame*, vol. 46, pp. 75–93, 1982.

[12] Richard Saurel, Fabien Petitpas, and Rémi Abgrall, "Modelling phase transition in metastable liquids: application to cavitating and flashing flows," *Journal of Fluid Mechanics*, vol. 607, pp. 313–350, 2008.

[13] Weixing Yuan and Günter H Schnerr, "Numerical simulation of two-phase flow in injection nozzles: Interaction of cavitation and external jet formation," *Journal of Fluids Engineering*, vol. 125, no. 6, pp. 963–969, 2003.

[14] Weixing Yuan, Jürgen Sauer, and Günter H Schnerr, "Modeling and computation of unsteady cavitation flows in injection nozzles," *Mécanique & Industries*, vol. 2, no. 5, pp. 383–394, 2001.

[15] Graham B Wallis, "One-dimensional two-phase flow," 1969.

[16] M-S Chung, S-B Park, and H-K Lee, "Sound speed criterion for two-phase critical flow," *Journal of sound and vibration*, vol. 276, no. 1-2, pp. 13–26, 2004.

[17] Lord Rayleigh, "On the pressure developed in a liquid during the collapse of a spherical cavity, VIII.," *The London, Edinburgh, and Dublin Philosophical Magazine and Journal of Science*, vol. 34, no. 200, pp. 94–98, 1917.

[18] Joseph Smagorinsky, "General circulation experiments with the primitive equations: I. the basic experiment," *Monthly weather review*, vol. 91, no. 3, pp. 99–164, 1963.

[19] Raad I Issa, "Solution of the implicitly discretised fluid flow equations by operator-splitting," *Journal of computational physics*, vol. 62, no. 1, pp. 40–65, 1986.

[20] Christopher E Brennen, *Cavitation and bubble dynamics*, Cambridge University Press, 2013.

[21] Boxiong Chen, Zachary Falgout, Mark Linne, and Michael Oevermann, "LES modelling of cavitation flow in a diesel injector nozzle," *International Conference on Multiphase Flow, 2016, Florence, Italy*.

[22] Stephen B Pope, "PDF methods for turbulent reactive flows," *Progress in Energy and Combustion Science*, vol. 11, no. 2, pp. 119–192, 1985.

[23] Stephen Bailey Pope, "A Monte Carlo method for the PDF equations of turbulent reactive flow," *Combustion Science and Technology*, vol. 25, no. 5–6, pp. 159–174, 1981.

[24] Luis Valiño, "A field monte carlo formulation for calculating the probability density function of a single scalar in a turbulent flow," *Flow, turbulence and combustion*, vol. 60, no. 2, pp. 157–172, 1998.

[25] J Dumond, F Magagnato, and A Class, "Stochastic-field cavitation model," *Physics of Fluids*, vol. 25, no. 7, pp. 073302, 2013.

3

Stochastic theory

3.1 Introduction

In the last chapter, we discussed how the vapor bubbles involved in the cavitation process can be modeled based on the the theory of single spherical bubble dynamics. However, as it has been mentioned, cavitation phenomenon involves highly complex bubble shapes and patterns such that no model at this stage could be expected to take all the aspects into consideration. Nonetheless, in this work we intend to improve the modeling of one of these important aspects, namely the stochastic fluctuation feature of vapor bubbles. Due to the turbulence commonly involved in realistic high pressure injector nozzles, vapor

bubble sizes undergo fluctuation. A close inspection on Eqn. (2.14) would reveal that, models based on only one volume fraction Eulerian field corresponds to only one radius at any spatial location in the computational domain, which is not sufficient to take stochastic fluctuation of bubble size (or volume fraction) into account. Such fluctuating behavior can be described by a stochastic variable, whose exact value is unknown or inaccessible. However, a function that describes the probability of the stochastic variable taking certain value, namely probability density function (PDF), can be used to provide a quantitative description of the stochastic variable. The approach that aims at solving PDF and thereby describing a stochastic fluctuation is commonly called PDF approach.

PDF approach was commonly applied in combustion applications and has traditionally been solved mostly through Lagrangian particle tracking (LPT). With the higher availability of computational resources, the interest of combustion community shifted from highly simplified and rudimentary cases (see e.g. [1, 2]) to cases that are more realisitc and computational resource demanding. As such, the difficulty involved in evenly distributing Lagrangian particles into processors makes it hard to apply LPT based approach on computationally "heavy" problems. Instead of tracking each Lagragian particle and extracting the PDF from informations carried on the particles, Valino in [3] represent each realization of the stochastic variable with an Eulerian field. When a number of Eulerian fields are put together, a PDF can be represented. Similarly, the evolution of each Eulerian field (which will be called stochastic field hereupon), when combined together, becomes the evolution of PDF. This is the esssence of the Eulerian Stochastic Field (ESF) method and will be discussed in details. Jones and Navarro-Martinez in [4] applied ESF approach to solve sub-grid PDF in a LES combustion computation and demonstrated the stochastic information of species mass fraction and temperature. In [5], Dumond et al. coupled the ESF method to a density based solver to model the cavitation phenomenon inside a venturi-like nozzle. The purpose of this work is to couple the ESF model to a pressure based solver (which is less demanding in computational power compared to density based solver and was discussed in details in the last chapter), in order to develop a computational tool that is more applicable to realistic

injector nozzles.

Now we start our discussion with a "formal" introduction to stochastic variables and probability density functions (PDF). The discussion is then transitted more specifically to the evolution of the PDF. The most general formulation, namely Kramers-Moyal equation will be derived first. Then we walk through some important constraints and reduce Kramers-Moyal equation to the more practical Fokker-Planck equation. Stochastic differential equations (SDE) will be introduced in the last part of the dicussion and how it relates to the Fokker-Planck equation will be discussed.

3.2 Stochastic variables and probability density function

The states of cavitation problems are often complex. The length scales involved in cavitation problems and the amount of bubbles involved makes it computationally immensly expensive to fully resolve. As it has been discussed in previous chapters, cavitation is a phenomena triggered by pressure change and is therefore a fast process as compared to boiling. The small time scales involved again make any attempt to fully resolve bubbles less than practical in engineering applications.

The concepts of probability and stochastics become helpful tools in situations where we do not know or have access to the complete state of a system Ξ under observation. Following the idea of stochastic theory, we consider the observable state as a stochastic variable ξ, the accurate value of which cannot be predicted. Nonetheless, the focus will then be put on accessing the probability of the stochastic variable ξ taking certain values. The stochastic variable ξ can be defined by taking all possible values into consideration and specifying the corresponding probability. The procedure described here leads to the definition of the probability density function (PDF) of the stochastic variable ξ.

3.2.1 PDF and its definition

Suppose we are given an amount of realizations of ξ. In order to calculate the probability of ξ taking certain values, we define a sample space which delimits the range of sample values. The sample space can then be discretized into an amount of smaller spaces, which are commonly refered to as bins. Then we observe the values of the realizations, count the times the value of realization fall into each of the bins. Dividing the count by the number of realizations, a probability of ξ falling into the corresponding bins is obtained. Lastly, in order to transform the discrete result we acquired from the procedure described above into a continuous one, the number of bins can be infinitely increased to make the PDF approach continuous. The procedure discribed above can be reformed into a stricter definition as follow:

Assuming N realizations of stochastic variable ξ are given,

1. Define a sample space $[X_-, X_+]$, which is considered as the space that includes all the values of ξ that can possibly appear. In order to treat this continuous space in a discrete manner, we discretize $[X_-, X_+]$ into N_x intervals. Each of the interval has a width $\Delta x = (X_+ - X_-)/N_x$.

2. For each i $(1 \leq i \leq N_x)$, count the number of times N_i when ξ values fall in the interval corresponding to x_i. Calculating N_i/N, we obtain the probability $p_\xi(x_i, t)$ of observing a value of ξ near x_i.

3. The integral of function p_ξ over $[X_-, X_+]$ will be $X_+ - X_-$. Thus, functions of multiple variables that are defined like this has shapes that are dependent on $X_+ - X_-$, which is inconvenient for mutual comparison. Therefore, a more convenient definition of PDF P_ξ of ξ, given by $N_i/(N\Delta x)$ is considered instead. Such P_ξ is standardized, namely its integral is equal to unity.

4. The above elements defines a discrete PDF. If we increase the number N to infinity and reduce Δx to infinitesimal, a continuous PDF is defined.

The fundamental properties of a continuous PDF P_ξ are summarized as follow:

$$P_\xi(x) \geq 0, \tag{3.1}$$

$$\int_{-\infty}^{\infty} P_\xi(x)dx = 1, \tag{3.2}$$

$$P_\xi(-\infty) = P_\xi(\infty) = 0. \tag{3.3}$$

3.2.2 Heaviside step function and Dirac delta function

The Heaviside step function, denoted here by H, is a discontinuous function named after Oliver Heaviside (1850-1925). Heaviside function and its derivative, delta function, are useful tools when considering PDF relevant problems. We digressto a discussion of them here before we further our discussion on PDF in the next section.

The Heaviside function is defined as follow:

$$H(x) = \begin{cases} 0, & \text{when } x < 0 \\ 1/2, & \text{for } x = 0 \\ 1, & \text{when } x > 0 \end{cases} \tag{3.4}$$

A picture of Heaviside step function can be found in Figure 3.1.

The Dirac delta function, or δ function, is a generalized function, or distribution that was introduced by the physicist Paul Dirac (1902-1984). It is defined as the derivative of the Heaviside function,

$$\delta(x) = \frac{dH(x)}{dx}. \tag{3.5}$$

A picture of Dirac delta function can be found in Figure 3.2.

Note that the ways to define step function, hence the ways to define delta function, are not unique. One possiblity would be

$$H(x) = \lim_{N\to\infty} \frac{1}{2}(1 + \tanh(Nx)) \tag{3.6}$$

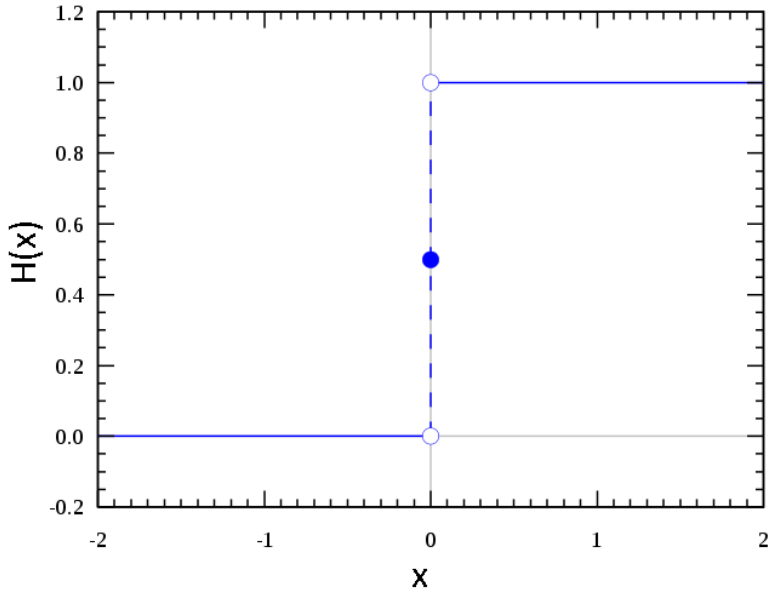

Figure 3.1: Heaviside function

Taking the derivative, we obtain the corresponding definition of δ.

$$\delta(x) = \lim_{N\to\infty} \delta_N(x) = \lim_{N\to\infty} \frac{N}{2\cosh^2(Nx)} \tag{3.7}$$

The figure shows that δ approaches zero for all $x \neq 0$, and it shoots up to infinity as $x \to 0$ when $N \to \infty$ (This is why the value of delta function at $x = 0$ is represented by an arrow in Figure 3.2). Therefore, δ function does not exist at $x = 0$, but integrals over it (which is frequently considered in the context of PDF and statistical moments) does exist anywhere in the space. For this reason, the delta function is called a generalized function or a distribution. Indeed, the normalization condition is satisfied:

$$\int_{-\infty}^{\infty} \delta(x)dx = \int_{-\infty}^{\infty} \frac{dH(x)}{dx}dx = H(\infty) - H(-\infty) = 1. \tag{3.8}$$

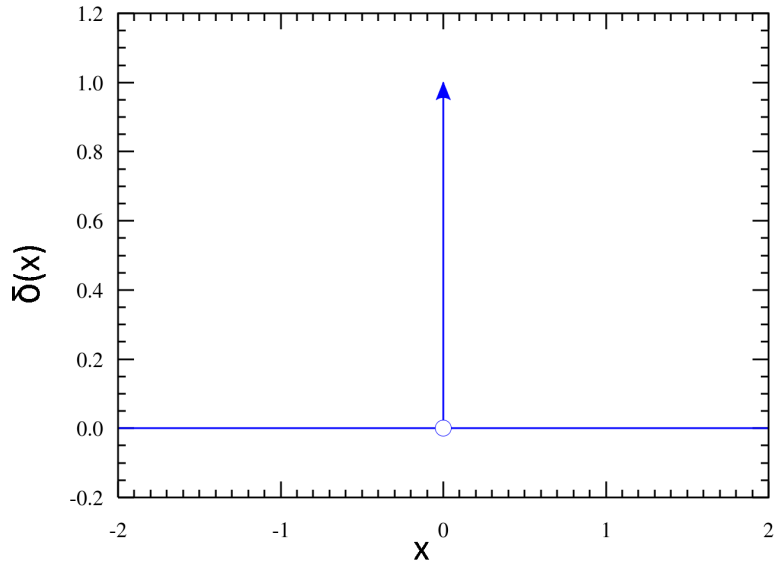

Figure 3.2: Schematic representation of the Dirac delta function.

3.2.3 PDF and delta function

Equipped with the discussion about Heaviside step function and Dirac delta function, we further reveal the relationship between PDF and delta function in this chapter. We start with the definition of the cumulative distribution function. The cumulative distribution function (CDF) of a stochastic variable ξ , or just distribution function of ξ , evaluated at x, is the probability that ξ will take a value not greater than x, i.e.,

$$F_{\xi}(x) = \frac{1}{N}\sum_{n=1}^{N} H(x - \xi^{(n)}), \tag{3.9}$$

where $\xi^{(n)}$ denotes the n_{th} realization of ξ . Also, it is worth mentioning that, in order to make the above equation valid in the strict sense, N needs to be increased till it approaches infinity and bin size along x axis has to be infinitesimal. However, in practical Monte Carlo simulations, N is usually only in-

creased to as large as computationally affordable and Δx reduced enough to produce a smooth PDF curve. Therefore, for the convenience of our discussion, we will not discern the differences of discrete and continuous definition of PDF and CDF any more hereupon. Also, if we denote the above ensemble average with angle brackets, and taking into consideration the temporal evolution of the stochastic variable,

$$F_\xi(x,t) = \frac{1}{N}\sum_{n=1}^{N} H(x - \xi^{(n)}(t)) = \langle H(x - \xi(t))\rangle \,. \tag{3.10}$$

The CDF of ξ $F_\xi(x,t)$ can be expressed as the integral of its PDF $P_\xi(x,t)$ as follows:

$$F_\xi(x,t) = \int_{-\infty}^{x} P_\xi(x,t)dx \tag{3.11}$$

Therefore, if we take the derivative through Eqn (3.10), by virtue of Eqn (3.5), we get,

$$P_\xi(x,t) = \langle \delta(x - \xi(t))\rangle \,. \tag{3.12}$$

Thus, we reach the conclusion that the PDF of a stochastic variable is equal to the ensemble average of its delta function over the sample space.

3.2.4 Extended PDF, correlations and conditional PDFs

The definitions of CDF and PDF in Eqn (3.10) and Eqn (3.12) can be extended easily to cover the case of multiple stochastic variables. In order to achieve this, we consider a vector of M stochastic variables $\boldsymbol{\xi}(t) = \{\xi_1(t), \xi_2(t), ..., \xi_M(t)\}$. Suppose we seek to calculate the probability of the combined event of seeing ξ at x at time t, and at x' at a different time t'. A two-point joint PDF can then be written as

$$P_{\boldsymbol{\xi}\boldsymbol{\xi}}(\boldsymbol{x}, t; \boldsymbol{x'}, t') = \langle \delta(\boldsymbol{x} - \boldsymbol{\xi}(t))\delta(\boldsymbol{x'} - \boldsymbol{\xi}(t'))\rangle \,. \tag{3.13}$$

With the knowledge of $P_{\boldsymbol{\xi\xi}}$ the ensemble average of an arbitrary function Q can be calculated by means of the relation

$$\langle Q(\boldsymbol{\xi}(t),t;\boldsymbol{\xi}(t'),t')\rangle = \int d\boldsymbol{x}d\boldsymbol{x'}Q(\boldsymbol{x},t;\boldsymbol{x})P_{\boldsymbol{\xi\xi}}(\boldsymbol{x},t;\boldsymbol{x'},t'). \tag{3.14}$$

If we integrate Eqn (3.13), we obtain a relation between one-point PDF and two-point PDF as follow:

$$P_{\boldsymbol{\xi}}(\boldsymbol{x},t) = \int d\boldsymbol{x'}P_{\boldsymbol{\xi\xi}}(\boldsymbol{x},t;\boldsymbol{x'},t'), \tag{3.15}$$

which can be proved by simply making use of the properties of Dirac delta function.

An important consideration in the joint statistics of multiple variables is whether they can be considered statistically mutually independent. This leads to the definition of a correlation and conditional PDFs. Specifically, a correlation is the measurement of the degree to which two stochastic variables are coupled. In many situations, we need to deal with the variables that are not mutually independent, therefore multiplication principle of PDF does not apply in such cases. Nevertheless, what we can do is to substitute the PDF of an independent variable with something called a conditional PDF. A more detailed discussion will be given on both correlation and conditional PDFs in this section.

Let us suppose we have two stochastic variables ϕ and ψ that are not necessarily mutually independent but are defined on the same sample space. A correlation can be defined as follow:

$$\rho_{\phi\psi} = \frac{\langle\phi\psi\rangle}{\langle\phi^2\rangle^{1/2}\langle\psi^2\rangle^{1/2}}. \tag{3.16}$$

Finding the bounds of $\rho_{\phi\psi}$ can lead to some useful conclusions. If we look at a non-negative functional F with an arbitrary parameter f, we have

$$F = \left\langle \left(\frac{\phi}{\langle\phi^2\rangle^{1/2}} + f\frac{\psi}{\langle\psi^2\rangle^{1/2}} \right)^2 \right\rangle = 1 + f^2 + 2f\rho_{\phi\psi} \geq 0. \tag{3.17}$$

F, as an emsemble average of some square terms, have to be greater than or equal to zero. The inequality above leads to

$$-\frac{1+f^2}{2|f|} \leq \rho_{\phi\psi} \leq \frac{1+f^2}{2|f|}, \tag{3.18}$$

since f is arbitrary. Since $\frac{1+f^2}{2|f|} \leq 1$, we have

$$|\rho_{\phi\psi}| \leq 1. \tag{3.19}$$

The above inequality is commonly known as **Cauchy-Schwartz inequality**. Later on we will refer to this inequality again to cancel out terms in the Kramers-Moyal equation and reach to the Fokker-Planck equation.

As it has been mentioned in the beginning of this section, when the stochastic variables are not statistically independent to each other, namely when the correlation is non-zero, the concept of conditional PDFs come into play. Specifically, a conditional PDF $P_{\boldsymbol{\xi}|\boldsymbol{\xi}}$ can be defined through its relationship with the joint PDF in Eqn (3.13):

$$P_{\boldsymbol{\xi}\boldsymbol{\xi}}(\boldsymbol{x}, t; \boldsymbol{x'}, t') = P_{\boldsymbol{\xi}|\boldsymbol{\xi}}(\boldsymbol{x}, t|\boldsymbol{x'}, t')P_{\boldsymbol{\xi}}(\boldsymbol{x'}, t'). \tag{3.20}$$

The conditional PDF $P_{\boldsymbol{\xi}|\boldsymbol{\xi}}$ represents the PDF of $\boldsymbol{\xi}(t)$ when $\boldsymbol{\xi}(t')$ is known to be $\boldsymbol{x'}$. Plugging in Eqn (3.20) into the RHS of Eqn (3.15), we have

$$P_{\boldsymbol{\xi}}(\boldsymbol{x}, t) = \int d\boldsymbol{x'} P_{\boldsymbol{\xi}|\boldsymbol{\xi}}(\boldsymbol{x}, t|\boldsymbol{x'}, t')P_{\boldsymbol{\xi}}(\boldsymbol{x'}, t'). \tag{3.21}$$

The above relation reveals the role of conditional PDFs in the evolution of PDFs. Given an initial PDF $P_{\boldsymbol{\xi}}(\boldsymbol{x'}, t')$ at time t', the dynamics of the system at a later time t is provided by the conditinal PDF $P_{\boldsymbol{\xi}|\boldsymbol{\xi}}(\boldsymbol{x}, t|\boldsymbol{x'}, t')$, which governs the evolution of the PDF. Later on we will run into an application of Eqn (3.21) in the derivation of the Kramers-Moyal equation, which is essentially a consideration of PDFs time evolution.

Conditional averages can be defined if we take a look at Eqn (3.20) and Eqn (3.14):

$$\langle Q(\boldsymbol{\xi}(t), t; \boldsymbol{\xi}(t'), t')\rangle = \int d\boldsymbol{x'} \, \langle Q(\boldsymbol{\xi}(t), t; \boldsymbol{\xi}(t'), t')|\boldsymbol{x'}, t'\rangle \, P_{\xi}(\boldsymbol{x'}, t'), \tag{3.22}$$

if we define the conditional average as

$$\langle Q(\boldsymbol{\xi}(t),t;\boldsymbol{\xi}(t'),t')|\boldsymbol{x'},t'\rangle = \int d\boldsymbol{x}\; Q(\boldsymbol{x},t;\boldsymbol{x'},t')P_{\boldsymbol{\xi}|\boldsymbol{\xi}}(\boldsymbol{x},t|\boldsymbol{x'},t'). \quad (3.23)$$

An important relation that will be used in the derivation of the Kramers-Moyal equation can be derived by virtue of Dirac delta function properties and Eqn (3.20):

$$\begin{aligned}
&\langle Q(\boldsymbol{\xi}(t),t;\boldsymbol{\xi}(t'),t')\delta(\boldsymbol{x'}-\boldsymbol{\xi}(t'))\rangle \\
&= \int d\boldsymbol{x} Q(\boldsymbol{x},t;\boldsymbol{x'},t')\,\langle\delta(\boldsymbol{x}-\boldsymbol{\xi}(t))\delta(\boldsymbol{x'}-\boldsymbol{\xi}(t'))\rangle \qquad (3.24)\\
&= \langle Q(\boldsymbol{\xi}(t),t;\boldsymbol{\xi}(t'),t')|\boldsymbol{x'},t'\rangle\, P_{\boldsymbol{\xi}}(\boldsymbol{x'},t').
\end{aligned}$$

3.2.5 Kramers-Moyal and Fokker-Planck equation

In the previous sections we discussed the PDF in details. Much of the derivations were kept to their simplest form with the purpose of supporting the derivation of evolution of stochastic variables in this section. Specifically, the derivation of the Kramers-Moyal equation, which we would walk through later, is essentially a Taylor expansion in time. As such, the conditional aspect of our PDF discussion becomes useful, because in the last section, it has been revealed that conditional PDFs governs the time evolution of PDF, when an initial PDF is given.

Kramers-Moyal equation have a theoretically infinite amount of terms from Taylor expansion, the modeling of which could have been highly complex. Fortunately, by considering the restraint from the Cauchy-Schwarz inequality, the majority of the terms will be zero, except for the first two. This basically simplifies the Kramers-Moyal equation into a Fokker-Planck equation.

The Fokker-Planck equation is a partial differential equation of PDF, the solution of which is mostly restricted to numerical in the majority of realistic applications. In practical simulations, we do not work on PDFs directly, but usually through solving a stochastic differential equation (SDE) that corresponds to the PDF. Specifically, the SDE can be more conveniently used to model the evolu-

tion of single field or particle, which goes well with the idea of Monte Carlo methods.

The Kramers-Moyal equation

In order to derive a transport equation for the PDF P_ξ, let us consider the PDF at time $t+\Delta t$. For simplicity, the derivations in this section will revolve around scalar stochastic variables. However, the conclusions can be extended easily so that they also apply to vectorial case. By virtue of Eqn (3.12),

$$P_\xi(x, t+\Delta t) = \langle \delta(x - \xi(t+\Delta t)) \rangle \,, \tag{3.25}$$

where Δt should be an infinitesimal time interval. It follows that the $\xi(t) - \xi(t+\Delta t)$ should be small, which makes it possible to do Taylor expansion at $x - \xi(t)$,

$$\begin{aligned} &\langle \delta(x - \xi(t+\Delta t)) \rangle \\ &= \langle \delta(x - \xi(t) + \xi(t) - \xi(t+\Delta t) \rangle \\ &= \sum_{n=0}^{\infty} \frac{1}{n!} \frac{d^n \delta(x-\xi(t))}{dx^n} [\xi(t) - \xi(t+\Delta t)]^n . \end{aligned} \tag{3.26}$$

The essence of ensemble averaging here is an arithmetic mean of the single realizations. Thus, if we isolate the $n = 0$ term in the RHS summation from the rest for each realization (not shown in the above equation) and take the arithmetic mean of them, we obtain the following relationship between PDF at t and $t + \Delta t$:

$$P_\xi(x, t+\Delta t) - P_\xi(x,t) = \sum_{n=1}^{\infty} \frac{1}{n!} \left(-\frac{d}{dx} \right)^n \langle [\xi(t+\Delta t) - \xi(t)]^n \delta(x - \xi(t)) \rangle \tag{3.27}$$

Applying Eqn (3.24), which we derived by the end of the last section, the RHS of Eqn (3.27) can be reformulated into

$$P_\xi(x,t+\Delta t)-P_\xi(x,t)=\sum_{n=1}^{\infty}\frac{1}{n!}\left(-\frac{d}{dx}\right)^n\langle[\xi(t+\Delta t)-\xi(t)]^n|x,t\rangle\,P_\xi(x,t). \tag{3.28}$$

Now we divide the LHS of Eqn (3.28) by Δt and let Δt approaches zero, we get an equation that is commonly known as the **Kramers-Moyal equation**:

$$\frac{\partial}{\partial t}P_\xi(x,t)=\sum_{n=1}^{\infty}\left(-\frac{\partial}{\partial x}\right)^n\alpha^{(n)}(x,t)P_\xi(x,t), \tag{3.29}$$

where the coefficients $\alpha^{(n)}$ are given by

$$\alpha^{(n)}(x,t)=\lim_{\Delta t\to 0}\frac{1}{n!}\frac{\langle[\xi(t+\Delta t)-\xi(t)]^n|x,t\rangle}{\Delta t}. \tag{3.30}$$

The Kramers-Moyal equation demonstrates once again that the conditional PDFs (more specifically, the conditional moment here) govern the evolution of PDF.

Constraint by the Cauchy-Schwartz inequality

To solve Eqn. (3.29), a number of coefficients need to be assessed. However, applying the Cauchy-Schwartz inequality as a constraint, we will soon find that most of the high order coefficients would have to be zero, which makes the consideration of the PDF evolution much easier.

It is obvious that all the derivation involved with Cauchy-Schwartz inequality applies to conditional means too. Therefore, if we take $\phi=(\Delta\xi)^{2m}$ and $\psi=(\Delta\xi)^{2n}$, where k and m are positive integers and $m<n$ (since m,n here are arbitrary integers, and the case when $k=m$ satisfies Cauchy-Schwartz inequality with equality of both sides and will not impose any constriant). Applying Cauchy-Schwartz inequality on the conditional means of ϕ and ψ, we have

$$\left\langle\Delta\xi^{m+n}|x,t\right\rangle\le\left\langle\Delta\xi^{2m}|x,t\right\rangle^{1/2}\left\langle\Delta\xi^{2n}|x,t\right\rangle^{1/2}. \tag{3.31}$$

Plugging the coefficients of Kramers-Moyal equation Eqn (3.30) into the above equation,

$$\left[(m+n)!\alpha^{(m+n)}\right]^2 \leq (2m)!(2n)!\alpha^{(2m)}\alpha^{(2n)}. \tag{3.32}$$

Firstly, let us assume $\alpha^{(2m)} = 0$. Then according to Inequality (3.32), $\alpha^{(m+n)}$ has to be zero, which implies all the coefficients with order higher than $2m$ have to be zero; Secondly, if we assume $\alpha^{(2n)} = 0$, then again $\alpha^{(m+n)}$ has to be zero, which implies all the coefficients with order lower than $2n$ need to be zero. Together, the combination of these two cases implies that if any of the even order coefficient is equal to zero, then terms $\alpha^{(m+n)}$ with arbitrary m and n would be eliminated. Since $1 \leq m < n$, $m+n \geq 3$, such elimination applies to any coefficient α with order higher than or equal to 3.

Now let us consider the case where we cannot assume any even order term to be zero. This implies the involvement of an infinite number of even order terms. Taking a look at Eqn (3.30), the time increment approaches zero in the definition of Kramers-Moyal coefficients. With an infinitesimal Δt, with a continuous sample path, we can expect the difference $\Delta\xi$ to be bounded, thus making it safe to neglect higher order terms α^m $(m = 3, 4, ...)$. Only when a jump process is considered, then the continuity of sample path may not remain valid. In such cases, higher order terms would need to be taken into consideration. However, for the applications involved in our turbulent cavitation process, such consideration will be safely excluded in our discussion.

The Fokker-Planck equation

Let us switch our focus back to the case of vectorial stochastic process $\boldsymbol{\xi}(t) = \{\xi_1(t), \xi_2(t), ..., \xi_M(t)\}$. Keeping only the first two terms, its corresponding extension of Kramers-Moyal equation reads:

$$\frac{\partial}{\partial t}P_{\boldsymbol{\xi}}(\boldsymbol{x},t) = -\frac{\partial}{\partial x_i}\alpha_i(\boldsymbol{x},t)P_{\boldsymbol{\xi}}(\boldsymbol{x},t) + \frac{\partial^2}{\partial x_i \partial x_j}\alpha_{ij}(\boldsymbol{x},t)P_{\boldsymbol{\xi}}(\boldsymbol{x},t). \tag{3.33}$$

The above equation is called a Fokker-Planck equation (Adriaan Fokker 1914, Max Planck 1917). The coefficients α_i and α_{ij} can be calculated in a generalzied form of coefficients in Eqn (3.29):

$$\alpha_i(\boldsymbol{x},t) = \lim_{\Delta t\to 0} \frac{\left\langle [\xi_i(t+\Delta t) - \xi_i(t)] | \boldsymbol{x}, t \right\rangle}{\Delta t} \tag{3.34a}$$

$$\alpha_{ij}(\boldsymbol{x},t) = \lim_{\Delta t\to 0} \frac{\left\langle [\xi_i(t+\Delta t) - \xi_i(t)][\xi_j(t+\Delta t) - \xi_j(t)] | \boldsymbol{x}, t \right\rangle}{2\Delta t}. \tag{3.34b}$$

Stochastic differential equations

The discussion so far has been focused on the evolution equation of the PDF. However, in practical simulations the PDF informations are rarely obtained through directly dealing with the PDF itself but through acquiring the informations of a number of realizations of the stochastic variables of interest. Let us suppose we postulate an evolution equation for the stochastic variables. If we can figure out a way to find out the corresponding PDF equation, then effectively we can obtain the PDF through solving the corresponding evolution equations of the stochastic variable. This is the reason why we shift the focus of our dicussion in this section from PDF evolution to constructing the stochastic differential equation that corresponds to it.

A general evolution equation for a vectorial stochastic variable $\boldsymbol{\xi}(t) = \{\xi_1(t), \xi_2(t), ..., \xi_M(t)\}$ can be written as

$$d\xi_i = a_i(\xi(s), s)dt + f_i dt, \tag{3.35}$$

where a_i is a term that governs the dynamics of the deterministic part of $\boldsymbol{\xi}$ evolution and f_i represents a stochastic force that generates fluctuations ξ'.

In the strict sense, both a_i may be dependent on all previous states $\xi(s)$, which would obviously hinder analysis of Eqn (3.35) and limit its application in practice. This independence on previous states is commonly known as "memory effect". Also, a characteristic correlation time of f_i, τ_f can be considered. The consideration of memory effects in a_i and finite correlation time τ_f could hinder

the analyses and limits the applications of Eqn (3.35) in practice and is beyond the scope of the discussion of our model. However, it is sufficient to know that a feasible choice of stochastic variables often makes the correlation time relatively small compared to the time scale of the problem considered. In line with this, the assumption of vanishing memory effect and infinitesimal correlation time will be adopted in the discussion that follows. Nevertheless, interested readers can find a more detailed discussion on such effects in [6]. For now, we restrict our attention to the following equation:

$$d\xi_i = a_i(\boldsymbol{\xi}, t)dt + b_{ij}(\boldsymbol{\xi}, t)dW_j, \tag{3.36}$$

where dW_j denotes the product of dt and the j^{th} component of a Wiener process (named in honor of Norbert Wiener, 1894-1964), which is a vectorial Gaussian process [7]. Thus, dW_j can be determined by

$$< dW_j >= 0, \tag{3.37a}$$

$$< dW_k(t)dW_l(t') >= \delta_{kl}\delta(t - t')dtdt'. \tag{3.37b}$$

which essentially means f_i at different time do not correlate to each other, which aligns with the infinitesimally small correlation time assumption.

Equipped with a fully constructed stochastic differential equation (SDE) (3.36), we can try to set up the connection between SDE and its corresponding PDF. Let us take a look at Eqn (3.29) and (3.30), we are now ready to calculate the Kramers-Moyal coefficients based on our SDE, Eqn (3.36):

$$\begin{aligned}\xi_i(t + \Delta t) - \xi_i(t) &= \int_t^{t+\Delta t} d\xi_i \\ &= \int_t^{t+\Delta t} dsa_i(\xi(s), s) + \int_t^{t+\Delta t} b_{ij}(\xi(s), s)dW_j(s) \\ &= a_i(\xi(t), t)\Delta t + b_{ij}(\xi(t), t)\Delta W_j(t),\end{aligned} \tag{3.38}$$

where $\Delta W_j(t)$ represents

$$\Delta W_j(t) = W_j(t + \Delta t) - W_j(t). \tag{3.39}$$

Please note that in the last step of the derivation in Eqn (3.38), the Ito definition of integration is adopted. More details on this type of integration will be discussed later. For now it is sufficient to regard it as a first-order forward integration over both time and stochastic contribution.

Performing the same integration over the increment of the Wiener process in Eqn (3.37) we obtain

$$\langle \Delta W_j(t) \rangle = 0, \tag{3.40a}$$

$$\begin{aligned} \langle \Delta W_k(t) \Delta W_l(t') \rangle &= \int_t^{t+\Delta t} \int_{t'}^{t'+\Delta t} \langle dW_k(s) dW_l(s') \rangle \\ &= \delta_{kl} \int_t^{t+\Delta t} ds \int_{t'}^{t'+\Delta t} ds' \delta(s-s') \\ &= \delta_{kl} \int_t^{t+\Delta t} ds [H(t'+\Delta t - s) - H(t'-s)] \\ &= \delta_{kl} \Delta t (1-k) \end{aligned} \tag{3.40b}$$

where $t' = t - k\Delta t$ $(k = 0, 1)$.

The relationship between SDE and Fokker-Planck equation is of high interest to us, because finding the corresponding SDE when we are given a PDF evolution enables us to solve PDF via solving SDE using Monte Carlo methods, which is the essence of this work. In fact, if we plug Eqn (3.38) into Eqn (3.34) and make use of relations (3.40)

$$\alpha_i(\boldsymbol{x}, t) = a_i(\boldsymbol{x}, t), \tag{3.41a}$$

$$\alpha_{ij}(\boldsymbol{x}, t) = \frac{1}{2} b_{ik}(\boldsymbol{x}, t) b_{jk}(\boldsymbol{x}, t). \tag{3.41b}$$

In the next chapter, we will derive the SDE equation for our cavitation problem using a simplified version of the above two relationships. It will be demonstrated that the Eulerian formulation of the PDF transport equation can be transformed into a Fokker-Planck equation, which, in turn, corresponds to a SDE, according to the discussion above. Then, an Eulerian field based Monte-Carlo type method (which will be referred to as Eulerian Stochastic Field (ESF) method) will be used to solve the SDE. Please see the detailed discussion in Chapter 4.

Bibliography

[1] Stephen Bailey Pope, "A Monte Carlo method for the PDF equations of turbulent reactive flow," *Combustion Science and Technology*, vol. 25, no. 5–6, pp. 159–174, 1981.

[2] Stephen B Pope, "PDF methods for turbulent reactive flows," *Progress in Energy and Combustion Science*, vol. 11, no. 2, pp. 119–192, 1985.

[3] Luis Valiño, "A field monte carlo formulation for calculating the probability density function of a single scalar in a turbulent flow," *Flow, turbulence and combustion*, vol. 60, no. 2, pp. 157–172, 1998.

[4] WP Jones and S Navarro-Martinez, "Large eddy simulation of autoignition with a subgrid probability density function method," *Combustion and Flame*, vol. 150, no. 3, pp. 170–187, 2007.

[5] J Dumond, F Magagnato, and A Class, "Stochastic-field cavitation model," *Physics of Fluids*, vol. 25, no. 7, pp. 073302, 2013.

[6] Stefan Heinz, *Statistical mechanics of turbulent flows*, Springer Science & Business Media, 2013.

[7] Crispin W Gardiner, *Handbook of stochastic methods*, vol. 3, Springer Berlin, 1985.

4

Stochastic numerical integration

4.1 Introduction

In this chapter we start our discussion from Monte Carlo type methods, which is the stochastic numerical method that is used in this work to simulate the PDF. The discussion is then transitted more specifically to Ito stochastic differential equation, then an extensive discussion on stochastic numerical integration schemes will be given.

4.2 Monte Carlo method

Monte Carlo methods are a broad class of computational algorithms that are used on a wide range of mathematical and physical problems. Several previous studies, e.g. [1–3] have applied Monte Carlo methods on the numerical solution of probability density functions (PDF). In essence, Monte Carlo methods are not concerned with capturing any particular realization of the solving variable, while stochastic quantities, such as mean value, are what Monte Carlo methods strive to capture. Through the random sampling process, a series of realizations are taken as representations of the variable, who stochastically resembles the solving variable. Therefore, stochastic variables such as mean value of the original variable can be estimated by the stochastic variables of the fields. These approaches rely on random sampling processes to obtain numerical results, whereas vastly different procedures are seen in different approaches. In [3], a Monte Carlo method is presented to simulate the finite difference solution of the PDF transport equation of turbulent reactive flows. By considering the joint probability density function of some of the flow variables, the closure problem associated with non-linearities in the Navier-Stokes equation is avoided. In reactive flows, the typically non-linear chemical source terms are closed through the application of PDF method. A complete set of statistical description of chemical species and thermodynamic properties can be accessed through the introduction of a joint PDF. The computational work involved in such method scales only linearly, in contrast to the power law dependence of a standard finite difference approach, with the number of independent variables of the joint PDF, therefore making it feasible for turbulent reactive flow with multiple species. In [4], an Eulerian field approach is designed to solve a dynamically scalar transport equation.

As has been pointed out in [5], cavitation flows are inherently stochastic because of the uncertainty involved in water quality (nuclei size and nuclei number PDF variance) and turbulence-cavitation interaction. In the modelling realm, an inspection on the cutting edge cavitation models [6] would reveal the non-linear nature of such models. Given the restriction on computational and experimen-

tal capacities, solving for instantaneous number and size of bubbles at specific locations would be neither economically feasible nor necessary for most flow applications, in which mean variables suffice for a reasonably accurate description of thermodynamic properties of the fluid. Therefore, a numerical tool that is capable of reproducing the statistical properties of the mean flow would be of higher practical interest. In the current work, a stochastic field method that resembles the methodology being used in [5] has been applied. Some fundamental numerical experiments are performed to testify the various stochastic integration schemes available. In [5], a standard forth-order Runge-Kutta scheme was applied to solve the deterministic part of the stochastic field, while the treatment of the stochastic part makes the overall accuracy only first order, despite the higher numerical robustness compared to regular first-order stochastic integration scheme. Although such scheme is consistent with the stochastic formulation, the wasted computational cost involved in the forth-order Runge-Kutta scheme makes such scheme less than optimal. Some ground-breaking studies on stochastic integration schemes have already been conducted in the mathematical realm, e.g. [7], [8]. A comparison of these stochastic numerical integration schemes is needed to obtain the necessary insight into them. The particularly interesting questions are, what are the theoretically consistent options, and how their performances compare in practice. In the current work, a Matlab code was developed to perform 1-D and 2-D stochastic simulations of sample problems, based on which we concluded that under the typical condition of using a relatively low number of realizations, the 2nd order stochastic Runge-Kutta (SRK2) method performs noticeably better than the 1st order Euler-Maruyama (EM1) method, and therefore was chosen as the tool for the numerical integration of the stochastic cavitation model developed and implemented in this thesis.

4.3 PDF and Ito stochastic differential equations

In [4], a novel PDF representation is developed, in which the description of PDF is based on an ensemble of Eulerian fields instead of Lagrangian particles, making the approach more efficient in parallel computations (see Chapter 3 for more elaborated explanations on this point). In line with the pure Eulerian approach presented in [4], state-of-the-art numerical algorithms for stochastic partial differential equations can be applied. While the method has been elaborated on in [4], a brief summary of the method will be given in this section in order to give a self-contained explanation of the method.

The transport equation of liquid volume fraction $\alpha_l(x,t)$ under the framework of LES can be derived from the general formulation Eqn. (2.16):

$$\frac{\partial \alpha_l}{\partial t} + u_j \frac{\partial \alpha_l}{\partial x_j} = D' \frac{\partial^2 \alpha_l}{\partial x_j \partial x_j} + S. \tag{4.1}$$

The convention of tensor notation is followed. Also u_j denotes a solenoidal velocity field, D' represents the turbulent diffusion coefficient and S denotes the source term coming from the cavitation model.

The time evolution equation for the PDF of α_l, with turbulent fluctuation modeled [4], can be written as follow:

$$\frac{\partial P_{\alpha_l}}{\partial t} + U_i \frac{\partial P_{\alpha_l}}{\partial x_i} + \frac{\partial}{\partial \psi}[S_v P_{\alpha_l}] = \frac{\partial}{\partial x_i}\left(D' \frac{\partial P_{\alpha_l}}{\partial x_i} \right), \tag{4.2}$$

where ψ is a variable in the sample space of P_{α_l} (Please note that it is not the same as α_l).

The main idea of the stochastic fields method is that, instead of solving the transport equation of the PDF itself, with some stochastic procedures, we come up with a series of Eulerian fields, the purpose of which is not to recover any particular realization of the scalar field α_l, but more importantly they share the same PDF with the scalar field α_l. In the above equation, we have gradient terms in both the spatial coordinates and the sampling space. Before applying the stochastic procedure on the PDF equation above, we would need to

reformulate it into a formula that is conducive to stochastic integration (i.e. a Fokker-Planck equation).

In Eqn. (3.33) in Chapter 3, we have given an introduction to Fokker-Planck equation (FPE). After a reduction on dimensionalities of the stochastic variable and all coefficients, a FPE of the liquid volume fraction PDF takes the following form:

$$\frac{\partial P_{\alpha_l}(\psi,t)}{\partial t} = -\frac{\partial}{\partial \psi}[a(\psi,t)P_{\alpha_l}(\psi,t)] + \frac{\partial^2}{\partial \psi^2}[b(\psi,t)P_{\alpha_l}(\psi,t)], \quad (4.3)$$

where P denotes the PDF of α_l. a, b are some arbitrary functions, which can be determined by the physical process that needs to be modeled.

In the last part of Chapter 3, the correspondence between FPE and Ito stochastic differential equation (SDE) have been demonstrated. More specifically, the relationships between the coefficients in FPE and SDE have been shown in Eqn. (3.41). The corresponding SDE of the above simplified FPE is:

$$\mathrm{d}\phi(t) = a[\phi(t),t]\mathrm{d}t + \sqrt{2b[\phi(t),t]}\mathrm{d}W(t) \quad (4.4)$$

where $W(t)$ is a Wiener process, the high dimensional version of which has been defined in Eqn. (3.40). A closer scrutinization on Eqn. (3.40) would reveal that the defition in Eqn. (3.40) is a necessary but not sufficient one of a Wiener process. However, a Wiener process can be reproduced using a continuous Gaussian stochastic process as follow:

- W(t)$\sim$N(0,t) for any t$\geq$0
- for any 0$\leq$s<t, [W(t)-W(s)]$\sim$N(0,t-s)

where N denotes normal distribution. We can place further limit on the second restriction:

$$\Delta W = \epsilon\sqrt{\Delta t}, \quad (4.5)$$

where $\epsilon \sim N(0,1)$. If we let Δt get infinitesimally small, we get,

$$\mathrm{d}W = \epsilon\sqrt{\mathrm{d}t}. \quad (4.6)$$

Equipped with the completely defined Wiener process we are ready to deal with the integral of the Ito SDE, namely

$$\phi(t) = \phi(t_0) + \int_{t_0}^{t} \mathrm{d}t' a[\phi(t'), t'] + \int_{t_0}^{t} \mathrm{d}W(t') b[\phi(t'), t']. \tag{4.7}$$

Having demonstrated how a SDE can be formulated when a FPE is given, we will now show that the PDF equation (4.2), can actually be transformed into a FPE. Put differently, all the spatial derivative terms in the PDF equation can be written into derivatives terms of the scalar. Such transformation reduces the multi-dimensional PDE into a one dimensional one, thus making the equation less expensive to solve. To start with, we will prove the following relation:

$$\frac{\partial P_{\alpha_l}}{\partial x_i} = -\frac{\partial}{\partial \psi}\left[\left\langle \frac{\partial \alpha_l}{\partial x_i} | \alpha_l = \psi \right\rangle P_{\alpha_l}\right], \tag{4.8}$$

where the angle brackets denote the ensemble averge of the contained quantity. Recall that in Chapter 3 we have proved that the PDF is equal to the ensemble average of δ function:

$$P_{\alpha_l}(\psi; x, t) = \frac{1}{N}\sum_{n=1}^{N} \delta[\psi - \alpha_l^n(x,t)] := \langle \delta[\psi - \alpha_l(x,t)] \rangle \tag{4.9}$$

It is well known, see e.g. [9], that the delta function has the following properties:

$$\delta(x - a) = \delta(a - x) \tag{4.10}$$

$$\delta^{(1)}(x - a) = -\delta^{(1)}(a - x) \tag{4.11}$$

where the superscript in brackets indicates a derivative and its order. Following

the above relations, we have:

$$\begin{aligned}
\frac{\partial P_{\alpha_l}}{\partial x_i} &= \frac{\partial \left\langle \delta(\alpha_l - \psi) \right\rangle}{\partial x_i} \\
&= \frac{\partial}{\partial x_i} \left(\frac{1}{N} \sum_{n=1}^{N} \delta[\alpha_l^n(x,t) - \psi] \right) \\
&= \frac{1}{N} \sum_{n=1}^{N} \frac{\partial}{\partial x_i} \delta(\alpha_l^n - \psi) \\
&= \frac{1}{N} \sum_{n=1}^{N} \frac{\partial \alpha_l^n}{\partial x_i} \frac{\partial \delta(\alpha_l^n - \psi)}{\partial \alpha_l^n} \\
&= -\frac{1}{N} \sum_{n=1}^{N} \frac{\partial \alpha_l^n}{\partial x_i} \frac{\partial \delta(\alpha_l^n - \psi)}{\partial \psi} \\
&= \frac{\partial}{\partial \psi} [\frac{1}{N} \sum_{n=1}^{N} \frac{\partial \alpha_l^n}{\partial x_i} \delta(\alpha_l^n - \psi)] \\
&= \frac{\partial}{\partial \psi} [\left\langle \frac{\partial \alpha_l}{\partial x_i} | \alpha_l = \psi \right\rangle P_{\alpha_l}]
\end{aligned}$$

Looking back at the PDF equation, the combined turbulent and molecular diffusion term requires applying the above relation twice:

$$\begin{aligned}
\frac{\partial}{\partial x_i}(D' \frac{\partial P_{\alpha_l}}{\partial x_i}) &= \frac{\partial D'}{\partial x_i} \frac{\partial P_{\alpha_l}}{\partial x_i} + D' \frac{\partial^2 P_{\alpha_l}}{\partial x_i \partial x_i} \\
&= \frac{\partial D'}{\partial x_i} \frac{\partial P_{\alpha_l}}{\partial x_i} - D' \frac{\partial}{\partial \psi} (\left\langle \frac{\partial^2 \alpha_l}{\partial x_i \partial x_i} | \alpha_l = \psi \right\rangle P_{\alpha_l}) \\
&+ D' \frac{\partial^2}{\partial \psi^2} (\left\langle \frac{\partial \alpha_l}{\partial x_i} \frac{\partial \alpha_l}{\partial x_i} | \alpha_l = \psi \right\rangle P_{\alpha_l})
\end{aligned} \tag{4.12}$$

The first term on the RHS can be dealt together with the convection term by applying the derivative variable exchange relation for another time, then we

get:

$$\begin{aligned}\frac{\partial P_{\alpha_l}}{\partial t} = \frac{\partial}{\partial \psi}[(U_i \left\langle \frac{\partial \alpha_l}{\partial x_i} | \alpha_l = \psi \right\rangle - \frac{\partial D'}{\partial x_i} \left\langle \frac{\partial \alpha_l}{\partial x_i} | \alpha_l = \psi \right\rangle \\ - D' \left\langle \frac{\partial^2 \alpha_l}{\partial x_i \partial x_i} | \alpha_l = \psi \right\rangle) P_{\alpha_l}] \\ + \frac{\partial^2}{\partial \psi^2}(D' \left\langle \frac{\partial \alpha_l}{\partial x_i} \frac{\partial \alpha_l}{\partial x_i} | \alpha_l = \psi \right\rangle P_{\alpha_l})\end{aligned} \tag{4.13}$$

The RHS of the above equation includes first and second order derivatives of the sampling variable of interest ψ. Therefore, the above equation, which is a transformed PDF equation, resembles the formulation of a FPE.

Recall that in Chapter 2, a volume fraction equation, Eqn. (2.16), which is mathematically identical to Eqn. (4.1), has been derived. Likewise, the volume fraction shares the same PDF transport equation. Therefore, a similar transformation from PDF equation to SDE can be applied, which leads to:

$$\begin{aligned}\mathrm{d}\alpha_l^n = \left[-u_i \frac{\partial \alpha_l^n}{\partial x_i} + D' \frac{\partial^2 \alpha_l^n}{\partial x_i \partial x_i} + S(\alpha_l^n) \right] \mathrm{d}t \\ + \sqrt{2D'} \frac{\partial \alpha_l^n}{\partial x_i} \mathrm{d}W.\end{aligned} \tag{4.14}$$

where the first term denotes the convection by filtered velocity field. D' denotes turbulent diffusion coefficient, which is given by the turbulence model. The unresolved velocity from our LES model kicks in via turbulent diffusion term and the stochastic term. $S(\alpha_l^n)$ is the source term that reflects the influence from the cavitation model. Please refer to Chapter 2 for more details. At this point, the SDE formulation of the liquid volume fraction equation has been developed and could readily be handled by the stochastic numerical integration schemes, which will be the focus of our discussion in the next section.

4.4 Stochastic integration schemes

Having shown the theoretical correspondence of the PDF equation and the Ito stochastic differential equation, the priority of our work now is to think about

what kind of numerical schemes we could possibly use to tackle a stochastic numerical integral. Out of intuition, it is natural to understand that the deterministic portions are not different with the normal integrals, and therefore can be treated with any typical numerical integration schemes, e.g., Runge-Kutta type methods. However, the existence of the Wiener process calls for a special type of numerical scheme because of the discontinuities it introduces.

The subject of SDE integration is a relatively young one with many intensive ongoing research. To be able to label the order of accuracy of SDE schemes as in conventional integration analysis, different definitions of accuracy would be needed, an elaboration which is beyond the scope of this work. Interested readers are refered to [10]. Here, two of the methods are selected in this work for further discussions:

- Euler-Maruyama method, a direct extension from traditional Euler first order scheme.
- Stochastic 2nd order Runge-Kutta method (SRK2).

Below we give a brief introduction to the Euler-Maruyama method and the higher order SRK2 method.

4.4.1 Euler-Maruyama method

The Euler-Maruyama method [11] is the simplest generalization of the Euler method of ordinary differential equation (ODE) to SDE. Consider the SDE

$$\mathrm{d}\phi(t) = a(\phi, t)\mathrm{d}t + b(\phi, t)\mathrm{d}W(t). \tag{4.15}$$

Suppose we solve the SDE on the interval $[0, T]$, with time step $\Delta t = T/N$, where N is the number of time steps, and initial condition $\phi(0) = \phi_0$. The **Euler-Maruyama approximation** to the true solution ϕ is the following series Y:

- set $Y_0 = \phi_0$

- recursive march the time

$$Y_{n+1} = Y_n + a(Y_n)\Delta t + b(Y_n)\Delta W_n \tag{4.16}$$

where $0 \leq n \leq N-1$, $\Delta W_n = W_{n+1} - W_n$

The advantage of such scheme is obviously its simplicity, although, not surprisingly, the accuracy of such method is low. And unfortunately the idea of such simple extension cannot be directly transplanted into higher order SRK schemes, as will be shown next. Despite of the disadvantages, it is a convenient method especially suitable for preliminary solution and comparison purposes.

4.4.2 2nd order stochastic Runge-Kutta method

Other than the first-order methods discussed above, A.Rößler in [12] has developed a range of Runge-Kutta schemes with 2nd order accuracy in the weak sense (for the definition of strong and weak accuracy, please refer to [10]), by different choices of coefficients and number of stages. A discussion on the general scheme and the order of accuracy would be beyond the scope of the current work. Here we adopt a specific scheme that is proposed in [7] and [8]:

$$Y_{n+1} = Y_n + \frac{1}{2}a(t_n, Y_n)\Delta t + \frac{1}{2}a(t_n + \Delta t, Y_n + a(t_n, Y_n)\Delta t + b\Delta W) + b\Delta W. \tag{4.17}$$

4.5 Numerical tests

Having all the theoretical background covered, some sample problems will be tested with the Euler-Maruyama and the SRK2 schemes. A finite difference code is written in matlab to perform these preliminary numerical experiments. In this section some results will be shown and discussed.

4.5.1 Test One

As in [3] and [4], we will solve a PDF transport equation that corresponds to a plug flow reactor configuration. With a simple molecular mixing model, the PDF equation becomes Equation (4.2) with the boundary conditions:

$$P(\phi;0,t)=\delta(\phi), \qquad \frac{\partial}{\partial x}P(\phi;1,t)=0$$

and the initial condition:

$$P(\phi;x,0)=\delta(1-\phi). \tag{4.18}$$

In order to apply Monte Carlo method, the transport equation for the PDF is transformed into the Eulerian field formulation:

$$\begin{aligned}\mathrm{d}\phi^n = &\left[-\frac{\partial\phi^n}{\partial x_i}+D'\frac{\partial^2\phi^n}{\partial x_i\partial x_i}-\frac{\omega}{2}(\phi^n- <\phi^n>)+a_1(1-\phi^n)\right]\mathrm{d}t \\ &+\sqrt{2D'}\frac{\partial\phi^n}{\partial x_i}\mathrm{d}W.\end{aligned} \tag{4.19}$$

The above equation is non-dimensionalized. The first term on the RHS is the convection by mean velocity, which aligns x_1 direction in this plug flow problem and is non-dimensionalized into 1. The constant values adopted in the current problem are:

$$a_1=3, \qquad \omega=20, \qquad D'=0.1.$$

For the above values, the scalar mean value has the following analytical solution:

$$\overline{\phi}(x)=1-\exp(-2.416x). \tag{4.20}$$

We obtained the result as in Figure 4.1. Both methods seem to have produced satisfactory results in this problem, while SRK seem to produce a result slightly closer than EM method. Indeed, when we check the 1-norm and 2-norm of the errors, we obtained Table. 4.1, which demonstrates that SRK method outperforms EM in this problem.

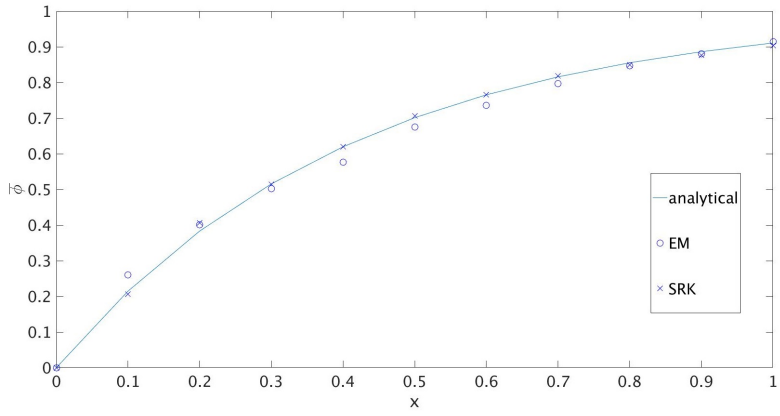

Figure 4.1: Test 1 for SRK and EM method, dt=0.01, dx=0.1, realizations=40

	EM	SRK
1-norm	0.2136	0.0645
2-norm	0.0810	0.0288

Table 4.1: Norms of the errors of EM and SRK method

4.5.2 Test Two

The second test resembles the one-dimensional problem in [7], a typical advection-diffusion equation with a stochastic forcing term:

$$\frac{\partial u}{\partial t} + v\frac{\partial u}{\partial x} - \nu\frac{\partial^2 u}{\partial x^2} = \sigma\frac{\partial W}{\partial x}, \tag{4.21}$$

where $x \in [0, 1]$, velocity $v = 0.6$, diffusion coefficient $\nu = 0.005$, $\sigma = 2.5$ subject to the initial condition

$$u(0, x) = \exp\left(-\frac{(x - 0.2)^2}{\nu}\right), x \in [0, 1] \tag{4.22}$$

and the boundary conditions

$$\begin{aligned} u(t,0) &= \frac{1}{\sqrt{4t+1}} \exp(-\frac{(-0.2-vt)^2}{\nu(4t+1)}), \\ u(t,1) &= \frac{1}{\sqrt{4t+1}} \exp(-\frac{(-0.8-vt)^2}{\nu(4t+1)}). \end{aligned} \tag{4.23}$$

It has the following analytical solution for the expected value of u

$$\overline{u}(t,x) = \frac{1}{\sqrt{4t+1}} \exp\left(-\frac{(x-0.2-vt)^2}{\nu(4t+1)}\right), x \in [0,1] \tag{4.24}$$

First, we would like to test the order of accuracy of the numerical schemes when the stochastic part of the equation is excluded, namely the accuracy involved in solving:

$$\frac{\partial u}{\partial t} + v\frac{\partial u}{\partial x} - \nu\frac{\partial^2 u}{\partial x^2} = 0 \tag{4.25}$$

Since the exact solution of u is known, and the error $\tilde{u}_{\Delta t} - u$ depends smoothly on time step Δt. Then an error coefficient D exists, such that

$$\tilde{u}_{\Delta t} - u = D(\Delta t)^p + O((\Delta t)^{p+1}). \tag{4.26}$$

If we compare the error involved with the time step Δt with the error involved with $\Delta t/2$, we get

$$\frac{\tilde{u}_{\Delta t} - u}{\tilde{u}_{\Delta t/2} - u} = \frac{D(\Delta t)^p + O((\Delta t)^{p+1})}{D(\Delta t/2)^p + O((\Delta t/2)^{p+1})} = \frac{D + O(\Delta t)}{D2^{-p} + O(\Delta t)} = 2^p + O(\Delta t). \tag{4.27}$$

Therefore, we have

$$\log_2\left(\frac{\tilde{u}_{\Delta t} - u}{\tilde{u}_{\Delta t/2} - u}\right) = p + O(\Delta t). \tag{4.28}$$

We can see that the 2^p in the above equation is essentially the rate of reduction of error, when time step is reduced by half. Thus, it is obvious that the p in the above equation is a measurement of order of accuracy involved with the estimation $\tilde{u}$.

Also, it is worth mentioning that the spatial discretization of convection and diffusion terms in Eqn. (4.25) also plays an important role in the accuracy of the numerical solution. If we move the convection and diffusion terms to the RHS of Eqn. (4.25), Eqn. (4.25) becomes an ordinary differential equation with a source term subjected to the errors involved in spatial discretization. Therefore, in this test problem, spatial grid size has to be reduced at a sufficient pace along with the time step in order to get the expected order of accuracy. In Table. 4.2, we can see that the order of accuracy, as formulated in Eqn. (4.28), converges to the expected values in both methods.

The results from the simulation, which are shown in Figure 4.2-Figure 4.4, agree well with the analytical solution. Here we are more interested in knowing how the two schemes behave with different time step and different number of realizations. As later on when calculating realistic problems, it is critical to control the computational cost.

Figure 4.2 and Figure 4.3 offer a comparison on the number of realizations. As is revealed in the 10000 realizations cases, at high number of realizations, both methods produce very satisfactory results. With a close inspection, SRK2 slightly outperforms Euler-Maruyama method at the range close to the peak. However, at a lower number of realizations, the SRK2 clearly achieves a higher level of agreement to the analytical expected value, especially at the peak region.

Figure 4.4 demonstrates the behavior of the two methods with different time step values. A trend similar to that with the number of realizations can be observed. Both of the methods agree very well with the analytical expected value, nonetheless the Euler-Maruyama gets a higher and higher deviation as compared to SRK2, as the time step is enlarged. Also, it can be observed that SRK2 captures the peak better than Euler-Maruyama method.

In summary, from the above figures, it is safe to conclude that with a refined time step and large number of realizations, both methods perform well. For realistic problems, in which the affordable computational cost limits the number

Time step\Order	RK	Euler
0.375	0.027357056	-2.493958563
0.1875	4.906621347	2.613280604
0.09375	1.85798613	1.098439156
0.046875	2.013216325	1.064692675
0.0234375	2.003496526	1.032936376
0.01171875	2.000880179	1.016683362
0.005859375	2.000220451	1.008405591
0.002929688	2.000055138	1.004220102
0.001464844	2.000013787	1.002114548
0.000732422	2.000003441	1.001058419
0.000366211	2.000000859	1.000529499
0.000183105	2.000000279	1.000264822
9.15527E-05	1.999998239	1.000132429
4.57764E-05	2.000011088	1.000066219
2.28882E-05	1.999980432	1.000033111
1.14441E-05	1.99995907	1.000016554
5.72205E-06	2.000300556	1.000008278
2.86102E-06	2.003399288	1.000004136
1.43051E-06	2.018844258	1.000002105

Table 4.2: Order of Accuracy of RK and Euler method

of realizations (in the current studies, the number of Eulerian fields), and when a larger time step is usually desirable, SRK2 has a considerably high advantage over the Euler-Maruyama method. Therefore, we selected the SRK2 method in the final implementation of the cavitation model.

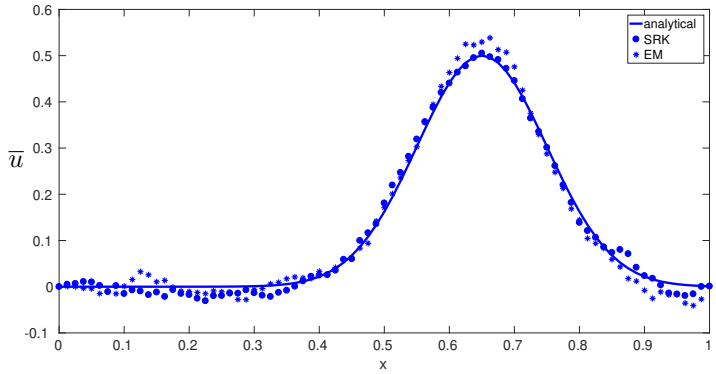

Figure 4.2: $\Delta t = 0.001s$, number of realizations: 1000

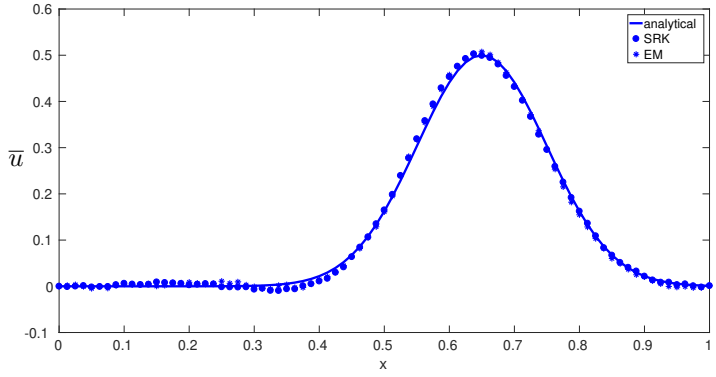

Figure 4.3: $\Delta t = 0.001s$, number of realizations: 10000

Bibliography

[1] Stephen B Pope, "PDF methods for turbulent reactive flows," *Progress in Energy and Combustion Science*, vol. 11, no. 2, pp. 119–192, 1985.

[2] BJ Delarue and SB Pope, "Calculations of subsonic and supersonic turbulent reacting mixing layers using probability density function methods," *Physics of Fluids*, vol. 10, no. 2, pp. 487–498, 1998.

[3] Stephen Bailey Pope, "A Monte Carlo method for the PDF equations of turbulent reactive flow," *Combustion Science and Technology*, vol. 25, no. 5–6, pp. 159–174, 1981.

[4] Luis Valiño, "A field monte carlo formulation for calculating the probability density function of a single scalar in a turbulent flow," *Flow, turbulence and combustion*, vol. 60, no. 2, pp. 157–172, 1998.

[5] J Dumond, F Magagnato, and A Class, "Stochastic-field cavitation model," *Physics of Fluids*, vol. 25, no. 7, pp. 073302, 2013.

[6] Christopher E Brennen, *Cavitation and bubble dynamics*, Cambridge University Press, 2013.

[7] Andreas Rößler, Mohammed Seaïd, and Mostafa Zahri, "Method of lines for stochastic boundary-value problems with additive noise," *Applied Mathematics and Computation*, vol. 199, no. 1, pp. 301–314, 2008.

[8] Mostafa Zahri, "On numerical schemes for solving a stochastic advection-diffusion," *International Journal of Pure and Applied Mathematics*, vol. 77, no. 5, pp. 681–694, 2012.

[9] Stephen B Pope, "Turbulent flows," 2001.

[10] Stefano M Iacus, *Simulation and inference for stochastic differential equations: with R examples*, Springer Science & Business Media, 2009.

[11] Klöden Platen, *Numerical Solution of Stochastic Differential Equations*, Springer Berlin, 1995.

[12] Andreas Rößler, "Runge–Kutta methods for Itô stochastic differential equations with scalar noise," *BIT Numerical Mathematics*, vol. 46, no. 1, pp. 97–110, 2006.

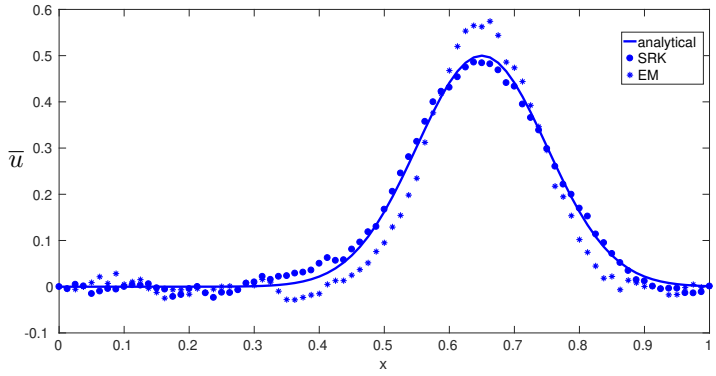

(a) $\Delta t = 0.01s$, number of realizations: 1000

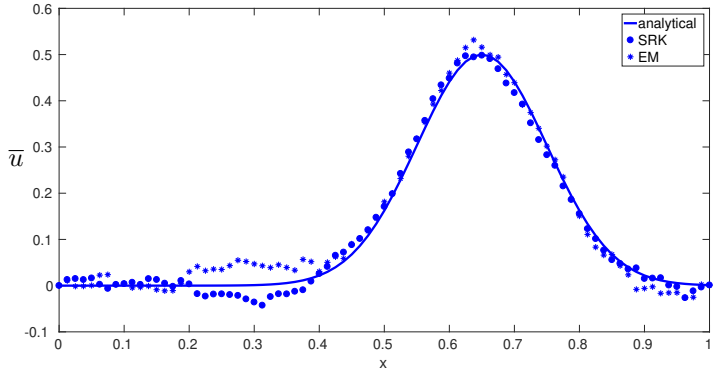

(b) $\Delta t = 0.001s$, number of realizations: 1000

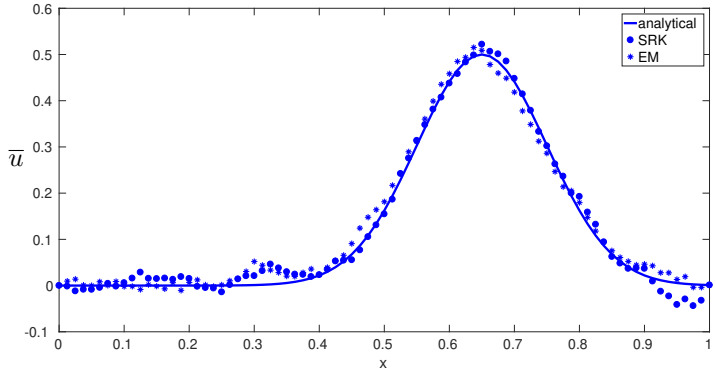

(c) $\Delta t = 0.0001s$, number of realizations: 1000

Figure 4.4: Comparison between SRK and EM with different time steps

5

Summary of papers

5.1 Introduction

In this chapter, we will first give some comments on the stability and computational cost of the stochastic model. Then, a brief summary of the papers published during the period of this project will be given. Also, along with the summary, the shortcomings and possible remedies involved with the publications will be discussed.

5.2 About the stability and computational cost

We did not experience any difficulty obtaining stable solutions in any of our ESF simulations. However, we expect more challenge from the stability perspective in simulations where the time steps are large. Because, the SRK2 integration scheme closely resembles the corresponding normal RK2 scheme in terms of stability. Nonetheless, in our cavitation simulations, where the typical time steps are on the scale of $1 \times 10^{-8}\,\mathrm{s}$ or $1 \times 10^{-9}\,\mathrm{s}$, numerical stability would not impose additional restriction.

In terms of the computational cost, our simulations with 50 stochastic fields demanded roughly 10 times the computational power that is needed for single volume fraction field simulations. However, a possible reason why the computational cost did not increase anywhere close to 50 folds is that the single volume fraction solver implementation used in our simulations is not fully explicit. Also, the pressure-velocity coupling might be the more time consuming part in single volume fraction solver, whereas the stochastic integration would clearly consume a dominating amount of computational time in the case of ESF simulations.

5.3 Paper I

LES modelling of cavitation flow in a diesel injector nozzle
Description: We performed the simulation of flows of a variety of fluids in a double-nozzle geometry of an academic injector, which corresponds to an experimental compaign in our department to measure the cavitation probability inside the same geometry.

Summary: We performed the simulation using a solver that closely resemble the Eulerian single volume fraction model. A model that was used in [1, 2] was applied to take mass transfer between liquid and vapor phase into account (For more details, please refer to Chapter 2). In addition, we take constant

speed of sound of the liquid and vapor phase into account in the solver we developed. The result presented in the paper showed qualitative agreement with the cavitation probability measurements. However, due to the limited computational time available, the turbulent flow patterns were not captured with the grid resolution by the time of the submission of the paper. To remedy this, simulations with finer grid resolutions were performed shortly after. In Figure. 5.1, the results from simulations using a more refined mesh (4 million nodes) are demonstrated. Snapshots of the volume fraction and velocity field in the mid-section of the double nozzle geometry were taken, in which turbulent behaviour of the flow was captured.

Also, given that this work was the first joint experiment and computational study in this series of cavitation study, for the purpose of model validation. A less complicated geometry and flow field should have been designed and investigated instead. It could involve looking into the flow and cavitation inside a single nozzle geometry. To make it even simpler, a single nozzle perpendicular to the volume sac could have been more feasible. Although this realization came to us in too late a stage in this study, it became useful and was reflected in the nozzle design in paper II.

5.4 Paper II

LES investigation with an Eulerian stochastic field cavitation model
Description: In this work, we applied the Eulerian Stochastic Field (ESF) cavitation model on a single nozzle injector geometry, which was designed for the an experimental study in Chalmers.

Summary: What we aimed to achieve in this work was: firstly, to make a comparison between our simulation result with the result from experimental study, by mainly comparing the mean volume fraction field with the images obtained from the experiments. Secondly, we would like to capture the temporal evolution of PDF. By the time of submission, the experimental images were not

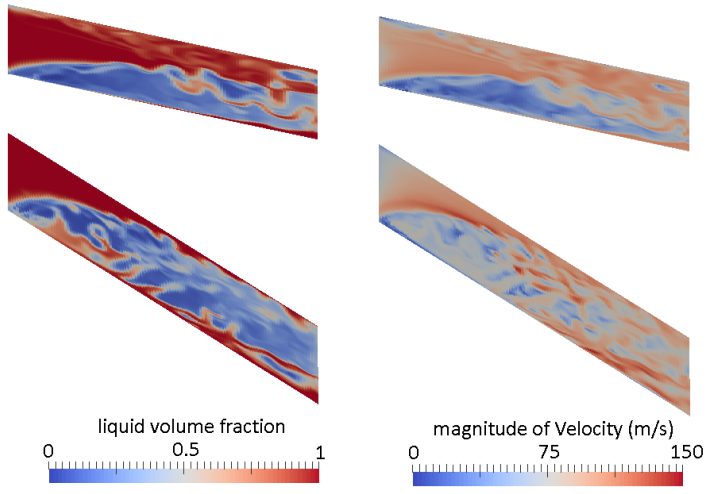

Figure 5.1: Liquid volume fraction and velocity field in the mid-section at time 0.02s, case dodecane with 45 bar injection pressure

finished, although our collegue reported observing super cavitation, which was confirmed in the simulation result. In Figure. 5.2, it can be observed that supercavitation was predicted by both Eulerian Stochastic Field model and single volume fraction solver. Turbulent behavior is captured by both of the models, and the sizes of the cavitation zones are quite similar in the simulation results of the two models. Figure. 5.3 demonstrated the temporal evolution of PDF at a position close to the wall.

It is also worth mentioning that, in the experimental study, when the sharp corners in the nozzle inlet were grinded a bit (the level of this could not be quantified due to the limitation of devices), making the corners a bit rounded, super cavitation would not be observed. This was an interesting observation and worth looking into from the persepctive of computational study. Unfortunately, it was not furthered due to the limited time. If the level of grinding can be quantified, the experimentally acquired images of nozzle flows could be used for the purpose of benchmark tests for computational models. It is our sincere

hope that researchers in the cavitation community would further the endeavour in this direction or in other fundamental studies on other benchmark cases in the future.

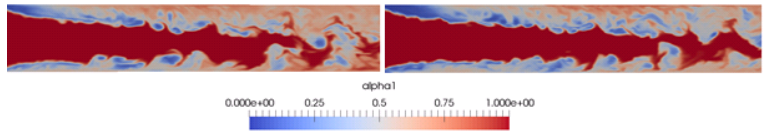

Figure 5.2: Instantaneous volume fraction from the stochastic field model on the left and single volume fraction solver on the right right

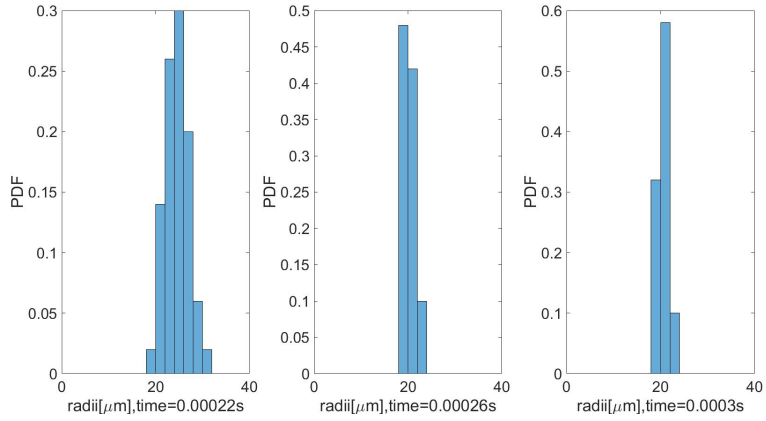

Figure 5.3: PDF evolution at a near wall position

5.5 Paper III

LES investigation of ECN spray G2 with an Eulerian stochastic field cavitation model

Description: In this work, a LES simulation in combination with our ESF cavitation model was performed to simulate the two-phase flow inside ECN spray G2 injector nozzle.

Summary: In previous studies associated with this project, LES simulations with ESF cavitation model have been performed in various academic throttle and injector nozzle geometries. However, the purpose of coupling the ESF model to a pressure based solver instead of a density based solver is to make ESF model more applicable to realistic injector designs in industrial practices, hence this work. The PDF of bubble sizes is captured and included in the resulting SAE conference contribution, see Figure. 5.4.

Due to a lack of measurements of pressure and velocity of in-nozzle flow, we included a comparsion between ESF model and single volume fraction solver results in the form of a pressure and velocity profile comparsion, which showed satisfactory agreement. The pressure profile comparison is shown in Fig. 5.5.

In the reviewing process, one of the reviewers questioned whether it was proper to ignore the role boiling might play in this study. Estimations of the time scales involved in the inertia driven vaporization (as modeled by Rayleigh-Plesset equation) and thermal effect were given and it was concluded that the cavitation is the dominating effect through the time bubbles are generated and convected to the downstream of injector nozzle holes under the temperature and pressure conditions of spray G2.

Also, the simulation in this work corresponds only to the "close" position of spray G2. Therefore, the level of vaporization downstream we observed in the simulation result was high. At the current stage, our ESF solver is not prepared to perform varing needle lift simulation, which requires the capacity to deal with moving boundaries. Future research and code developement works dedicated to this aspect could be of great practical interest.

It is worth mentioning that a talk associated with this work was given in the ECN 5.8 web meeting by the author. The high level of curiosity and interest from the ECN community towards this model make the author grateful and feel promising that more studies focusing on the in-nozzle flow would become available in the near future.

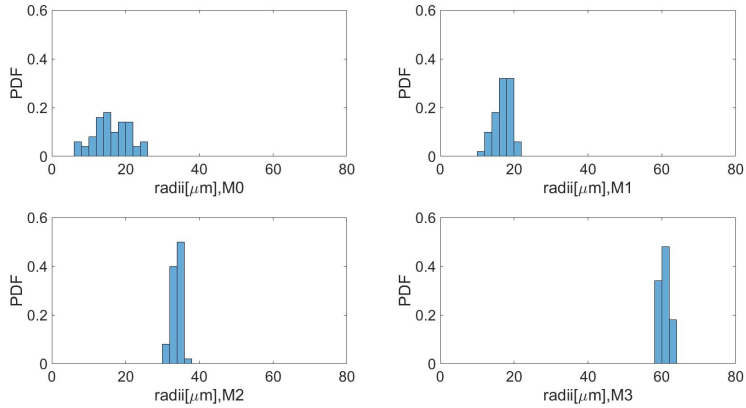

Figure 5.4: PDF of bubble radii at different spatial locations.

5.6 Paper IV

An Eulerian stochastic field cavitation model coupled to a pressure based solver

Description: In order to test the ESF model, the simulation in this work was performed, the results of which were compared with a previous computationala study on the throttle geometry using single volume fraction solver.

Summary: This is our first work after the completion of ESF model development. A correlation between the geometric shape of the vapor zone and vortex structure was observed in this study, which proved that turbulence could interact strongly with cavitation, rendering LES simulation crucial to cavitation studies (RANS based models might fail to capture the effect of vortices on cavitation). The correlation observed in this study could have been significantly harder to find in a more complex geometry, as the vorticity and cavitation patterns could be too complicated to make such observation. Thus, from another perspective, we can see that studies focusing on simple geometries could provide unique insights that could be otherwise inaccessible or prone to be missed out in complex studies.

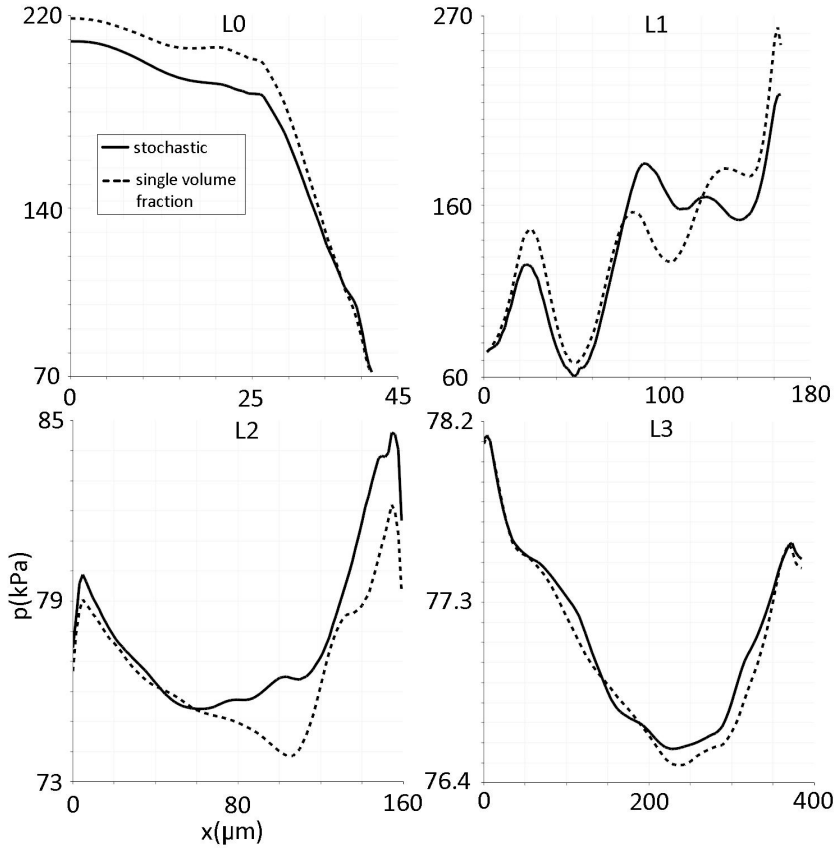

Figure 5.5: Time averaged pressure (kPa) along L0, L1, L2, and L3 as predicted by sotchastic model (solid lines) and single volume fraction solver (dash lines)

Clip shots of cavitation zones at different longitudinal positions predicted by stochastic model and single volume fraction solver are shown in Fig. 5.6. As it can be seen, although the geometrical shape of cavitation zones in the two results are similar, the difference in the shapes indicates that the mass transfer model used in this work is highly sensitive to the difference in pressure predicted by the two models (Several liquid volume fractions are solved in ESF model, thus bringing a disturbance to pressure solution, which, in turn, might

cause difference in liquid volume fraction solution).

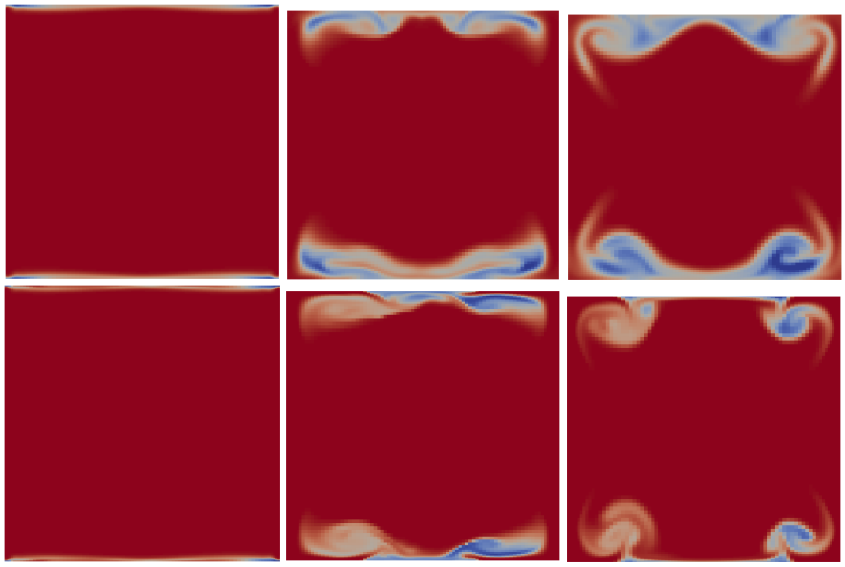

Figure 5.6: Volume fraction profiles from stochastic solver (top) and single volume fraction VOF solver (bottom) at S0 (left), S1 (middle), S2 (right). Colors are scaled to the values in the respective clip to give a clear demonstration of the volume fraction pattern.

Also, using smaller time steps in the simulation, we observed smaller cavitation zones as compared to [3]. Future studies on the sensitivity of cavitation on temporal and spatial resolutions could possibly provide better guidelines for cavitation simulations.

Bibliography

[1] Weixing Yuan, Jürgen Sauer, and Günter H Schnerr, "Modeling and computation of unsteady cavitation flows in injection nozzles," *Mécanique & Industries*, vol. 2, no. 5, pp. 383–394, 2001.

[2] Weixing Yuan and Günter H Schnerr, "Numerical simulation of two-phase flow in injection nozzles: Interaction of cavitation and external jet formation," *Journal of Fluids Engineering*, vol. 125, no. 6, pp. 963–969, 2003.

[3] Mireia Altimira and Laszlo Fuchs, "Numerical investigation of throttle flow under cavitating conditions," *International Journal of Multiphase Flow*, vol. 75, pp. 124–136, 2015.

6

Possible directions for future works

6.1 Possible directions for future works

Although we have completed the discussion on the contributions and the shortcomings of the works involved with the publications in the last chapter, here we still feel the necessity to show some of our thoughts on the topic of cavitation and the proposed stochastic model as a summary of this work, which will hopefully provide some possible directions for future works on cavitation.

First off, although the work presented here in this thesis has provided proof that ESF model can be used to compute PDF of vapor bubbles in complex geometries, the discussions here could have greatly benefited from some validations

on the PDF level. However, to our best knowledge, experimental works measuring the PDF of vapor bubbles were lacking during the testing phase of our model. The majority of the experimental works available focus their emphasis on the correspondence between experimentally observed vapor bubble zones and computationally predicted cavitation zones, as indicated by the liquid or vapor volume fraction. A rough match in the length of such cavitation zone alongside the flow passage is often used as an indicator of the level of match, which is a rather crude way for the purpose of validations. As such, at the current stage of cavitation research, finding help from experimental data is obviously difficult. And future experimental works targeting the measurements of the PDF of vapor bubbles will clearly be of great help to the validation of stochastic computational models.

Direct numerical simulations could possibly provide the information needed for the validation, it would certainly be computationally too expensive on a full scale industrial injector nozzle. However, fundamental DNS works could possibly validate the PDF information on simplified geometries. Nonetheless, since the purpose of this work is to demonstrate that the combination of incompressible solver and ESF method could be applied in computations with complex geometries, we have to leave this possibly non-trivial work to the future research efforts.

Another interesting way to seek for potential validation could be to make comparison against well established Lagrangian models. In fact, Lagrangian models might benefit from a mutual comparison as well. Ebrahim et al. in [1] has developed a hybrid mixture bubble model for cavitation simulations. The problem with validating ESF with Lagrangian models, however, would be that Lagrangian models will probably be less effective computationally than Eulerian models, and hence incur even higher computational cost than what ESF model would need. But again, such comparison could probably be done on a simpler geometry in the future.

Secondly, some extensions on the Sauer-Schnerr model could easily make the model more applicable to cases that involve large difference in inlet temperature

and temperature of the downstream (which is probably common under realistic working conditions of injection needles). Also, the applicability of the ESF solver could be further boosted if dynamic mesh features can be implemented in the solver. We hope that future works would carry out such extensions and bring the potentional of the ESF model into full play.

Bibliography

[1] Ebrahim Ghahramani, Mohammad Hossein Arabnejad, and Rickard E Bensow, "Realizability improvements to a hybrid mixture-bubble model for simulation of cavitating flows," *Computers & Fluids*, vol. 174, pp. 135–143, 2018.

Appendices

A

OpenFOAM implementation

A.1 Introduction

In the previous chapters, the theoretical and algorithmic details have been discussed in preparation for the code implementation of the current study. This chapter focus specifically on the details involved in the coding aspect. Firstly, an introduction and general perspectives will be given on the numerical tool that will be used, namely OpenFOAM (Open Field Operation and Manipulation) and the major standard solvers pertinent to the current study, with the particular aim of connecting the standard implementation with the theoretical background. Secondly, we will briefly walk through the code structure of the

cavitation models that has already been available in the standard release, in order to lay a perceptional foundation for the implementations of stochastic module. In the last section, a demonstration of the implementation of the stochastic model, as well as the underlying stochastic integration library will be given.
Much unlike in the previous chapters, where theory presents heavily, the contents of this chapter are organised with the aim that is twofold: First is to show the code implementation of the model in a reader-friendly way; second is to provide an example on how to harness the available code snippets in OpenFOAM package to fulfil our purpose in practice. It has always been a sincere hope of the author that more pragmatic tutorials of OpenFOAM would become available to the users, so that they could handle the code with ease, and such convenience would hopefully in turn attracts more users into the open source community. Because the collaboration under the spirit of open source is, in the author's opinion, the most effective way of fostering the development of CFD.

A.2 OpenFOAM and its standard solvers

Computational Fluid Dynamics (CFD) has been well established since its earliest applications in meterology in the early 20's. With the increasing computational power becoming available at a lower price, the application of computational models has become an indispensable part of the studies on the respective physical problems in both academical and industrial practices. Several commercial CFD packages, e.g., Star-CD, Fluent, CFX, FIRE, have accomplished great success and have long been available in the market. However, with the ever increasing complexities and amount of details involved in the problems of interest, reducing the overhead involved in the licence costs has also become increasingly more important for CFD users. In line with this concern, OpenFOAM (Open Field Operation and Manipulation) has attracted a substantial amount of attention from both academical and commercial users since its first release in 2004. Researchers in the multiphase flow area have been using

OpenFOAM extensively since some of the earliest release, and a range of well developed solvers are readily available in the OpenFOAM standard releases. The ongoing OpenFOAM implementation and debugging effort in the multiphase area by the community has made OpenFOAM an excellent platform for high-level solver development. Some major solvers that are worth mentioning are (Lagrangian particle based solvers are not included here due to the lower relevance to the current work):

- interFoam [1], solver for 2 incompressible, isothermal immiscible fluids using a VOF (volume of fluid) phase-fraction based interface capturing approach. Its multiple fluids counterpart multiphaseInterFoam has adopted the same approach.
- twoPhaseEulerFoam, solver for a system of 2 compressible fluid phases with one phase dispersed, e.g. gas bubbles in a liquid including heat-transfer.
- cavitatingFoam, transient cavitation code based on the homogeneous equilibrium model from which the compressibility of the liquid/vapour "mixture" is obtained.
- interPhaseChangeFoam [2], solver for 2 incompressible, isothermal immiscible fluids with phase-change (e.g. cavitation). Uses a VOF (volume of fluid) phase-fraction based interface capturing approach.

Since the purpose of the project is to develop an Eulerian stochastic model in the VOF framework, and the state-of-the-art simplified Rayleigh-Plesset model [3] [4] has already been implemented in interPhaseChangeFoam, interPhaseChangeFoam is selected as the basis of the further development of the current work. In the following sections, we will first briefly talk about the pressure equation involved in the interPhaseChangeFoam solver, and then focus mainly on the implementation details of the new model, namely the SRK2 stochastic integration module, and the stochastic model library. The details of the code provided in this section is based on Foam extended 3.1, minor variations may apply to

different releases.

A.3 A review on interPhaseChangeFoam

Before delving into the implementation of the stochastic model in this work. It is necessary to talk about the base solver involved in this work, namely interPhaseChangeFoam. Particularly, we argued that the equation

$$\nabla \cdot \vec{U} = \frac{\rho_v - \rho_l}{\rho} \frac{d\alpha_l}{dt} \tag{A.1}$$

in Chapter 2. In the discussion below, the corresponding code snippets will be demonstrated.
Let us first have a look at pressure equation of the interFoam solver, in pEqn.H, we can find

```
......
        fvScalarMatrix pdEqn
        (
            fvm::laplacian(rUAf, pd) == fvc::div(phi)
        );
......
```

In the pressure solving loop. And it is a common practice in OpenFOAM implementation to apply divergence constraint from the mass conservation equation to the momentum equation. In [5], a semi-discretised form of the momentum equation is used:

$$a_p \boldsymbol{U_p} = \boldsymbol{H}(\boldsymbol{U}) - \nabla p \tag{A.2}$$

where a_p denotes the diagonal entries of the discretized momentum equation and $\boldsymbol{H}(\boldsymbol{U})$ represents the summation of the product of the off-diagonal matrix of $\boldsymbol{U}$ and the explicit terms of $\boldsymbol{U}$ that come from time discretisation. $\boldsymbol{H}(\boldsymbol{U})$ is typically treated explicitly to avoid heavy computational cost involved in matrix

inversion (or in more practical terms, matrix decompositions). $\boldsymbol{U}$ can then be expressed as

$$\boldsymbol{U_p} = \frac{\boldsymbol{H(U)}}{a_p} - \frac{1}{a_p}\nabla p \tag{A.3}$$

For the purpose of theoretical discussion, the difference between cell values and face values will not be discerned here. As such, if we apply zero divergence condition to the above equation, we have

$$\nabla \cdot \Big(\frac{1}{a_p}\nabla p\Big) = \nabla \cdot \Big(\frac{\boldsymbol{H(U)}}{a_p}\Big) \tag{A.4}$$

which corresponds exactly to code snippet presented in the beginning of this section. In the pEqn.H file of interPhaseChangeFoam, the corresponding pressure matrix is assembled as follow:

```
......
fvScalarMatrix pdEqn
        (
            fvc::div(phi) - fvm::laplacian(rUAf, pd)
          + (vDotvP - vDotcP)*(rho*gh - pSat)
  + fvm::Sp(vDotvP - vDotcP, pd)
        );
......
```

Obviously, the first two terms represents what we have already seen in interFoam solver, the last two terms, however, accounts for the RHS of divergence constraint (A.1).

A.4 Implementation of SRK2

A good practice of OpenFOAM development involves selecting the available code pieces to start with. And as was mentioned before, the deterministic part of the stochastic integration closely resembles the normal numerical integration. As an open source project with some past development, OpenFOAM has

an ODE library that serves this purpose. In the ODE library, the RK directory contains the components for a 4th order Runge-Kutta integration. A few steps can be taken to modify the ODE libraries into the stochastic integration library we need:

- Take a copy of the original ODE library, then remove the numerical methods that are irrelevant to our purpose. In foam extended 3.1, Euler, KRR4, SIBS directories should be removed. Meanwhile corresponding changes in Make files have to be made.
- Tailor down the 4th order RK scheme into a 2nd order RK. This mainly involves deleting many integration coefficients defined in the first few lines of RK.C file, and those in the constructor. Then remove the excessive integration stages in function "solve". A compile and test on the 2nd order RK method at this point is highly recommended before proceeding.
- Implement the stochastic part. The class "Random" is a random number generator in OpenFOAM that can be used to perform a Gaussian sampling (cachedRandom class is not kept in foam extended 3.1, but it can also be used if available). The stochastic contribution should then be added into the corresponding lines of the "solve" function.

Note that keeping the code structure of ODE library enables an easy potential addition of other numerical integration schemes into the library. Another scheme can be easily implemented independent on the existing SRK2 components.

A.5 Implementation of stochastic model

The stochastic ODE library (which will be referred to as stchODE from now on, following the naming in the implementation) only solves the stochastic ODE, but a module that assembles the equation is still needed. In standard inter-

PhaseChangeFoam solver, the equation of volume fraction exist in alphaEqn.H, and it is numerically solved in the MULES solver which is located in /finiteVolume/fvMatrices/solvers. What we need to achieve here is to build a substitution for alphaEqn.H which will be solved by our stchODE library.
The question that follows during the implementation was: "What are the essential features of the stochastic model that are fundamentally different from those of the interPhaseChangeFoam?" In author's opinion, implementation-wise the differences lie in two aspects:

- Stochastic method solves realisations of volume fraction on multiple Eulerian fields instead of just one. So we need to find where the Eulerian field is defined in interPhaseChangeFoam, and add the multi-fields feature into that structure for our application.
- The solving of stochastic method relies on the stchODE module we have developed, which means an ideal target template should be some class that resorts to ODE library for solution. That template class can then be modified to assemble our stochastic equation, and call stchODE for solution.

The following two sections contain brief discussions that support these two aspects with details on the implementation level. For better clarity, readers are recommended to refer to the corresponding code snippets.

A.5.1 stochasticPhaseChangeTwoPhaseMixture

First off, we have to locate the Eulerian field in interPhaseChangeFoam. It is obvious that in creaetFields.H of interPhaseChangeFoam,

```
volScalarField alpha1
(
    IOobject
    (
        "alpha1",
```

```
            runTime.timeName(),
            mesh,
            IOobject::MUST_READ,
            IOobject::AUTO_WRITE
        ),
        mesh
    );
```

declares the Eulerian field. Then we notice that in the declaration of phaseChangeTwoPhaseMixture,

```
...
    autoPtr<phaseChangeTwoPhaseMixture> twoPhaseProperties =
        phaseChangeTwoPhaseMixture::New(U, phi, "alpha1");
...
```

A character string is passed to the runTime selection (of the cavitation models). Digging deeper into the class phaseChangeTwoPhaseMixture, we find no trail of alpha1 inside the phaseChangeTwoPhaseMixture class itself. However, a closer inspection on phaseChangeTwoPhaseMixture.H reveals that,

```
class phaseChangeTwoPhaseMixture
:
    public twoPhaseMixture
{
...
```

could have make the manipulation of alpha1 possible for phaseChangeTwoPhaseMixture (such manipulations can be found in any of the cavitation models, e.g., in SchnerrSauer.C), through the inheritance from twoPhaseMixture structure. Indeed, after locating the twoPhaseMixture files (in /src/transportModels /incompressible/incompressibleTwoPhaseMixture), in twoPhaseMixture.H, we find the following line in the class declaration:

```
...
        const volScalarField& alpha1_;
```

```
...
```

which hints at the chance that twoPhaseMixture might communicate with the alpha1 in createFields.H through the above reference. This can easily be confirmed by the constructor in twoPhaseMixture.C:

```
...
    alpha1_
    (
        U_.db().lookupObject<const volScalarField>
        (
            alpha1Name
        )
    ),
...
```

so the lookupObject function searches for the alpha1 field, and returns the reference to twoPhaseMixture.
Having understood the principle of how phaseChangeTwoPhaseMixture works, we can start to build the block for our purpose. In order to operate on the multiple Eulerian fields, the PtrList structure is used in our current implementation. In author's implementation, stochasticTwoPhaseMixture.H

```
...
        PtrList<volScalarField> alpha1_;
...
```

And in the constructor of stochasticTwoPhaseMixture in the corresponding C file, the number of the fields is first passed to the constructor, and then a mechanism that identify, name, and initialise the Eulerian fields is implemented.

```
...
    forAll(alpha1_, i)
    {

        char buffer[8];
```

```
sprintf(buffer,"%d",i);

Foam::word stringI(buffer);

IOobject header
(
    "alpha1_" + stringI,
    U_.mesh().time().timeName(),
    U_.mesh(),
    IOobject::NO_READ
);

// check if field exists and can be read
if (header.headerOk())
{
    alpha1_.set
    (
        i,
        new volScalarField
        (
            IOobject
            (
                "alpha1_" + stringI,
                U_.mesh().time().timeName(),
                U_.mesh(),
                IOobject::MUST_READ,
                IOobject::AUTO_WRITE
            ),
            U_.mesh()
        )
    );
```

```
        }
        else
        {
            alpha1_.set
            (
                i,
                new volScalarField
                (cd
                    IOobject
                    (
                        "alpha1_" + stringI,
                        U_.mesh().time().timeName(),
                        U_.mesh(),
                        IOobject::NO_READ,
                        IOobject::AUTO_WRITE
                    ),
                    alpha1Mean_
                )
            );
        }
    }
...
```

Other auxiliary functionalities, such as obtaining the mean value of Eulerian fields, are also implemented in stochasticPhaseChangeTwoPhaseMixture. Meanwhile, the cavitation models, for instance, SchnerrSauer.C require some modification to fit into the multi-field structures. However, since the work involved in these aspects are fairly straight forward but scattered in the code, they will not be covered here due to the limited volume of this instruction. Interested readers are highly encouraged to refer to the code for more details. While the application of such mechanism will be touched upon again in the next section, where the equation is assembled.

A.5.2 stochasticModel and stochasticSolver

As has been mentioned before, since we designed our stchODE library in a way largely similar to the ODE library. So for the equation assembling purpose, it is natural to seek for a structure in foam that resorts to ODE for solution. Some code pieces in foam provides such examples, e.g. chemistryModel and chemistrySolver in thermophysicalModels. So the design of stochastic model vaguely follows the pattern in chemistryModel in the sense that stochasticModel provides necessary functions that interface with ODE library, such as nEqns, derivatives, and jacobian, and stochasticSolver inherits stochasticModel, unwraps it, and calls the stchODE solver for solution in the end. In the following content of this section, we would briefly walk through the final implementation of stochasticModel and stochasticSolver and commentate as it is due.

stochasticModel.H

stochasticModel inherits stchODE class:

```
...
class stochasticModel
:
    public stchODE
...
```

Such inheritance guarantees that stochasticModel, or any derived class of it would be able to call the solver in stchODE. In fact we would see later that the this is done by stochasticSolver, who includes stochasticModel as a member.

```
...
    autoPtr<stochasticPhaseChangeTwoPhaseMixture>
    twoPhaseProperties_;

    transportModel& twoPhaseTransport_;
```

```
...
```

These references and pointer are basically a replication of those in the createFields.H of interPhaseChangeFoam, as the transport properties are necessary for the update of properties, when the new solution becomes available.
As mentioned previously,

```
...
        virtual label nEqns() const;

        virtual void derivatives
        (
            const scalar t,
            const scalarField& y,
            scalarField& dydt
        ) const;

        virtual void stochasticTerm
        (
            const scalar t,
            const scalarField& y,
            vectorField& stch
        ) const;

        virtual void jacobian
        (
            const scalar t,
            const scalarField& y,
            scalarField& dfdt,
            scalarSquareMatrix& dfdy
        ) const;
...
```

Are the functions that interface with stchODE library. Here, they are virtual functions but not pure virtual ones because in stochasticMode.C they will be loaded with our stochastic equations.

stochasticModel.C

As shown in the last section,

```
...
    twoPhaseProperties_
    (
        stochasticPhaseChangeTwoPhaseMixture::New
        (
            NoR,
            U,
            phi,
            alpha1Name
        )
    ),
    twoPhaseTransport_
    (
        dynamic_cast<transportModel&>
        (
            twoPhaseProperties_()
        )
    ),
...
```

These are the handles for the properties' update.

```
...
Foam::label Foam::stochasticModel::nEqns() const
{
    return twoPhaseProperties_
```

```
        ->alpha1Mean_.internalField().size();
}
...
```

We will pass all the internal nodes of the Eulerian fields to stchODE for solution.

```
...
void Foam::stochasticModel::derivatives
(
    const scalar t,
    const scalarField &y,
    scalarField& dydt
) const
{

    volScalarField yc(twoPhaseProperties_->alpha1Mean_);

    volScalarField detRHS
    (
        IOobject
        (
            "dydt",
            mesh_.time().timeName(),
            mesh_,
            IOobject::NO_READ,
            IOobject::NO_WRITE,
            false
         ),
        mesh_,
        dimensionedScalar("zero",dimless/dimTime,0.0)
    );

    yc.internalField() = y;
```

```
    yc.correctBoundaryConditions();
...
```

The derivatives function provides the deterministic portion of the RHS source. The reason why we build volScalarField yc here is because, we need the solution of the old step (both internalField and the boundary condition) later on to calculate the deterministic source. However, the interface of virtual function derivatives has to follow the same pattern as that in stchODE, and the solution of the old step can only be seen through the reference of scalarField y (which means boundary conditions are missing). So here we recover the old solution by taking a new field yc, which is declared and initialised with the mean solution field. It follows that yc would get the same boundary conditions as the mean field, which actually are the same boundary conditions with solution fields of each realisations. And once yc has taken y, the boundary conditions is updated, then the yc becomes the full old solution field.

```
...
    const surfaceScalarField& phiRef
        = mesh_.lookupObject<surfaceScalarField>("phi");

    Pair<tmp<volScalarField> > vDotAlphal
        = twoPhaseProperties_->vDotAlphal(yc);

    const volScalarField& vDotvAlphal = vDotAlphal[1]();

    detRHS = (
                //- Diffusion
                fvc::laplacian
                (
                    turbulence_->nuEff(),
                    yc
                )
                //- Convection
```

```
                - fvc::div
                  (
                      phiRef,
                      yc
                  )
                + fvc::Sp(fvc::div(phiRef),yc)
                  //- sgs molecular mixing
                  //  In the explicit source function,
                  //  only the first input get returned.
                - fvc::Su
                  (
                      scalar(0.5)
                    * (yc - twoPhaseProperties_->alpha1Mean_)
                    / tsgs(),
                      yc
                  )
              );

    dydt = detRHS.internalField();
    dydt += vDotvAlphal.internalField()*yc.internalField();
...
```

These portion assembles the deterministic source. We can see that all the fvc operations work on volScalarField, not scalarField, and this justifies our roundabout representation of the old solution field. Since dydt has to be scalarField, it takes back only the internalField information from detRHS. The last line represents the contribution from the cavitation model. A similar mechanism has been used in function stochasticTerm to recover the full solution field, which needs no further elaboration.

stochasticSolver

Since the content of stochasticSolver is rather straightforward, we would not go over the files line by line. However it is worth mentioning that,

```
...
    PtrList<volScalarField>& alpha1 = stchModel_.alpha1();

    forAll(alpha1,i)
    {

        scalarField& ci = alpha1[i].internalField();

        stchODESolver_->solve
        (
            stchModel_,
            t0,
            t0 + dt,
            ci,
            deltaT
        );
...
```

extracts the internal nodes values and pass them to the stchODE solver. If we have a look at the stchODE solver (The reader is recommended to check out the stchODESolver.C file in the directory: /applications/solvers/interPhaseChangeFDFFoam /stchODE/stchODESolvers/stchODESolver as continue reading),

```
...
void Foam::stchODESolver::solve
(
    const stchODE& ode,
    const scalar xStart,
    const scalar xEnd,
```

```
    scalarField& y,
    scalar& h
)
{
    const label MAXSTP = 10000;

    scalar x = xStart;

    for (label nStep=0; nStep<MAXSTP; nStep++)
    {
        ode.derivatives(x, y, dydx_);

        ode.stochasticTerm(x, y, stch_);
...
        solve(ode, x, y, dydx_, stch_, h);
...
```

Comparing the interface of the above function and that of stochasticSolver::solve function (Note that there is another solve function that has a different interface. It is a different function, following C++ syntax), it becomes obvious that stchODESolver::solver takes the internalField values of each of the alpha field from stochasticSolver::solve, pass them to ode.derivatives and ode.stochasticTerms, which are in fact the corresponding functions in stochasticModel that we have covered in the previous section. These functions return the deterministic and stochastic source in the form of `dydx_` and `stch_`, which are then passed to the core stchODE solver. When the solution is completed, back in stochasticSolver.C file,

```
...
        stchODESolver_->solve
        (
            stchModel_,
            t0,
```

```
            t0 + dt,
            ci,
            deltaT
        );

        alpha1[i].correctBoundaryConditions();
...
```

The ci, which refers to the internalField of alpha[i] gets updated, and the last line updates the boundary conditions of alpha[i]. When the loop of i is finished, the solution of all Eulerian fields is completed.

Bibliography

[1] Suraj S Deshpande, Lakshman Anumolu, and Mario F Trujillo, "Evaluating the performance of the two-phase flow solver interfoam," *Computational science & discovery*, vol. 5, no. 1, pp. 014016, 2012.

[2] ST Miller, Hrvoje Jasak, DA Boger, EG Paterson, and A Nedungadi, "A pressure-based, compressible, two-phase flow finite volume method for underwater explosions," *Computers & Fluids*, vol. 87, pp. 132–143, 2013.

[3] Weixing Yuan, Jürgen Sauer, and Günter H Schnerr, "Modeling and computation of unsteady cavitation flows in injection nozzles," *Mécanique & Industries*, vol. 2, no. 5, pp. 383–394, 2001.

[4] Weixing Yuan and Günter H Schnerr, "Numerical simulation of two-phase flow in injection nozzles: Interaction of cavitation and external jet formation," *Journal of Fluids Engineering*, vol. 125, no. 6, pp. 963–969, 2003.

[5] Hrvoje Jasak, *Error analysis and estimation for the finite volume method with applications to fluid flow*, Ph.D. thesis, Imperial College London (University of London), 1996.